Department of Precision and Microsystems Engineering

Gear Repair using Laser Metal Deposition

M. Bons

Report no : 2020.019
Coach : Dr. C. Ayas
Professor : Prof.dr.ir. A van Keulen
Specialisation : ED
Type of report : MSc. thesis
Date : 30-06-2020

Gear Repair

using Laser Metal Deposition

M. Bons

TU Delft

GBS

Gear Repair

using Laser Metal Deposition

by

M. Bons

to obtain the degree of Master of Science

at the Delft University of Technology,

to be defended publicly on Tuesday June 30, 2020 at 14:00 AM.

Student number:	4153804	
Supervisor:	Dr. C. Ayas	TU Delft
	Ir. D. A. van Ekeren	GBS Gearbox Services
Project duration:	December 11, 2017 – June 30, 2020	
Thesis committee:	Prof. dr. ir. A. van Keulen	TU Delft
	Dr. V. Popovich	TU Delft
	Dr. C. Ayas	TU Delft

This thesis is confidential and cannot be made public until June 30, 2022.

TU Delft

GBS

Preface

I would like to use this opportunity to express my gratitude to everyone who supported me throughout the course of this long-term project.

Firstly, I am grateful to my thesis supervisor Dr. Can Ayas of the TU Delft. His thorough reviewing and constructive criticism have contributed a lot during the project. In addition, I would like to thank the professors and my fellow students at the TU Delft, who took time to listen to my presentations and gave helpful remarks.

Furthermore, this research was funded by GBS Gearbox Services. I would like to thank the company for giving me the time and resources to do all the necessary tests. I want to thank Alber van Ekeren and Jan de Koning in particular for giving me the in-depth analysis and guidance during this long period.

Last but not least, I wish to express my sincere thanks to my family and friends for their endless mental support, encouragement and patience. This would not have been possible without them.

M. Bons
Delft, June 2020

Abstract

The urge for more sustainable and cost-efficient repair methods for damaged parts is growing every day. On the other hand, laser metal deposition (LMD) is gaining momentum. This flexible technique, where material is added in a layer-by-layer fashion with a minimal heat input offers solutions for a wide range of production and repair purposes. Especially restoration or replacement of large and complex high-performance parts with long production times could profit from these developments. Industrial gears are certainly such type of parts. Occasionally, unforeseen tooth breakage of gears occurs, often leading to the replacement of the parts. No reliable repair techniques have emerged yet, due to the desired material properties and the uneven distributed hardness seen in carburized gears. This study was initiated to examine the feasibility of LMD for the repair of industrial gears with the goal to reduce both material waste and down time while retaining or exceeding the required mechanical performance.

The research problem is broken down into smaller focus areas by an extensive gear tooth analysis. Based on the different types of loading in a gear tooth, the tooth is divided in two main areas: a hard and wear resistant tooth flank at the location of contact and remainder of the tooth, covering the core and root.

The initial part of the research is focused on finding the best suitable material and deposition parameters to ensure the desired mechanical properties of the core and a good bonding of the structure to the gear. Multiple deposition parameters are varied followed by destructive and non-destructive testing. It was found that the mechanical properties of deposited structures Inconel 718 and its bonding to a carburized substrate can be adjusted by accurately selecting the deposition parameters. Large differences in outcome were obtained by changing the deposition direction between each layer and tuning of the shielding gas flow rate. When comparing the mechanical properties of the deposited structure and a common gear steel it is seen that the ultimate tensile strength and yield strength do not match the desired properties. Nonetheless, a superior impact toughness was observed.

In further investigation the effects on the mechanical behavior of a deposited tooth structure were studied by altering the thermal cycle during and after deposition. The tests are performed on a specially developed static load testing setup. The results show a negative correlation between the interpass temperature and both the yield and ultimate tensile strength. This effect is attributed to a lower cooling rate during solidification at higher interpass temperatures. Moreover, it is found that the addition of a deposited hard flank material induces an increase in yield strength of the total structure. Despite the fact that this flank material showed brittle fracture the structure did not fail, proving a superior core ductility.

Ultimately, the results of a deposited tooth with hard flanks and built on a case hardened base were compared to a case hardened gear tooth that was manufactured according to the regular production method. It is found that the deposited structure exhibits significantly lower yield strength. Nonetheless, the superior ductility of the newly deposited tooth structure in the presented work is considered as a promising method for future gear repair.

Nomenclature

Chemical elements

Al	Aluminium
B	Boron
C	Carbon
Cr	Chromium
Fe	Iron
Mn	Manganese
Mo	Molybdenum
Nb	Niobium
Ni	Nickel
Si	Silicon
Ti	Titanium

Acronyms

AM	Additive Manufacturing
CAD	Computer-Aided Design
DOF	Degrees Of Freedom
DLD	Direct Laser Deposition
HAZ	Heat Affected Zone
HPSTC	Highest Point of Single Tooth Contact
ISO	International Organization for Standardization
LENS	Laser-Engineered Net Shaping
LMD	Laser Metal Deposition
LPSTC	Lowest Point of Single Tooth Contact
PWM	Pulse Width Modulation
SLS	Selective Laser Sintering

Contents

1

Introduction

In a world where environmental value starts to play a bigger role each year, it is worth thinking about changing certain habits in the production world. In 2010, industrial activities caused approximately 30% of global Greenhouse gas emission [1]. Lately, greener industries arise and the recycling of products is becoming more common nowadays. However, developments in the metal producing and manufacturing area have had little modification until the late 1990's, leaving their approach outdated. Luckily, in the past few decades, more innovations and new manufacturing techniques have started to emerge. Especially in repair and recycle a lot of improvement has been made.

Now imagine when a fully working mechanism, no matter how small or big, breaks down. Hundreds of years ago, the mechanism would simply be replaced. Then later on people started to look for a more efficient way to fix the problem by replacing broken parts; the old parts were taken out, new ones were built and put back in. Although this made quite a difference, more improvement was possible: instead of throwing away a broken part by a new one, it was taken out, inspected and repaired; time, material and energy is saved.

The definition of part repair is restoring a malfunctioning part back to its initial or operational acceptable state. This usually involves the replacement of a damaged or worn-out piece of a part. Traditionally this is done by removing a fraction of the old material so a new layer of material can be added, usually with the use of so called Additive Manufacturing (AM), which refers to manufacturing technologies where material is deposited - usually layer upon layer - to build an object from a CAD model. With the above mentioned growing environmental awareness this way of repairing has led to the era of remanufacturing [2]; repairing, replacing and redesigning old parts so they match or even outperform the broken products. In the last case, one may think about adding a more wear resisting layer on part surfaces subject to heavy wear for example. Study has shown that using AM techniques as a repair method usually have environmental benefits over the manufacturing of new parts [3, 4]. With the contemporary environmental awareness this led to the urge for a wider application of this repair technique. For instance, turbine blades were brought back to their original state using AM with excellent bonding characteristics [3, 5]. Remanufactured engine shafts even outperformed the original ones [6, 7] after the deposition of a new and more wear resistant layer.

A rather unexplored area that could benefit from this growing repair industry are industrial gears. Industrial gears can be found in drive trains of ships and cranes and production is a very time-consuming process due to the high standards regarding performance and durability. A case of unforeseen destructive damage, such as tooth breakage, could cause a lot of downtime, leading to high costs and waste material. It is favorable to investigate the possibilities to quickly repair such damage instead of producing a new part. Older repair techniques such as arc welding did not seem suitable for the repair of industrial gears, since with these processes typically an enormous amount of heat input in the part is involved [8]. Higher heat input leads to a large volume of heat affected material, also known as the heat affected zone (HAZ). Preferably the HAZ should be kept as small as possible for products such as industrial gears, since excessive heating leads to unwanted changes in mechanical properties of low alloy steels such as tempering effects. However, last 20 years gave more insight on AM techniques. The use of laser as a heat source ensures that the energy can be focused right at the place where it is desired. With this highly controllable heat input new repair processes emerged. One of

those processes is called laser metal deposition (LMD), a manufacturing method that could be described as laser guided metal based 3D-printing. With LMD, material can be selectively added by blowing powder into a moving melt pool which is initiated and maintained by a laser beam. A small downside of the technique is the low production speed compared to arc welding. Nevertheless does the controllability of the deposited material with a relatively low heat input make it a very suitable option for the repair of industrial gears.

This research is focused on investigating the possibilities to replace a complete tooth of an industrial gear using LMD. The main goal is to achieve a static mechanical behavior of a 3D printed tooth similar to that of the original one. This is done by a thorough literature survey, followed by a multi-step research approach, investigating different deposition parameters.

This project is done in association with GBS Gearbox Services, a company with over 10 years of experience in gearbox repair and metalwork. Their main goal is to improve production and overhaul techniques. In 2015, the company invested in a LMD setup. At first, the main purpose for this installation was the repair of worn out shafts and bearing housings. Although a lot of knowledge is gained with respect to single layer repair process, they are still unable to repair heavily damaged gears. This research is initiated by the growing interest in applying the LMD installation for gear restoration purposes.

2

Background

The aim of this research is to apply LMD as a repair technique for industrial gears. This combines mechanics and material science, bringing in many challenges. A complete understanding of the problem requires sufficient background knowledge on both topics. The acquired background knowledge gathered by a thorough literature survey is presented in this chapter, followed by a risk analysis of the application of LMD for gear repair.

2.1. Industrial Gears

When the wheel was invented, humanity discovered the benefits of rotational motion transfer. This motion transfer was best done by allowing two wheels to come into contact. However, in this case only low torques and speeds are preferred since the transfer is based on friction contact. Exceeding the friction force will cause slip and therefore causes the output to be significantly smaller than the input due to losses. To counteract this effect, sticks where attached in the outer rim of the wheels, the first pin gears were developed. Animal driven mechanisms and even mills were invented, all to make human life easier. Later, the pins where removed and grooves got carved onto the wheel, generating the well-known gears we heavily rely on today. This technique was spreading rapidly and more and more applications emerged. However, wear appeared to play a big role in the lifetime of gears. Due to the circular movement of a gear the teeth were sliding against each other, creating a lot of wear during the transmission of high torques. Tooth profiles were adjusted so the relative translational motion between tooth flank during power transmission was minimized. This converted most of the sliding contact into a rolling contact, limiting the forces acting on a tooth flank to mainly compressive forces. This significantly improved the efficiency, lifetime and performance of the gears when used in ideal circumstances. When eventually metal gears were produced, the possibilities seemed limitless. High torques could be passed through and different types of gears where invented; from simple but robust spur gears to complete mechanisms such as differentials and planetary gears.

2.1.1. Design

Many ways for gear applications come with a wide variation of gear types available. The main design properties for an industrial gear are strength, dynamic load resistance and surface durability. Most of these goals can be achieved by proper geometric design and material selection.

Geometry

Industrial power transmissions are characterized by high torques and low speeds, this often leads to gears with large dimensions. Another important aspect in industry is production costs. As a result, simplicity in manufacturing is required. To minimize the amount of designs for a gear the flank shape of the teeth is standardized. Instead of a straight flank, the gears have a so called involute shape, as shown in Figure 2.1a. The curved geometry creates a constant pressure angle (typically 20°) between two gears, contributing to a

smooth power transmission. Another great benefit of this design is the load distribution across two pairs of teeth at certain points during a load cycle. It is known that the tensile stresses at the root of the tooth are maximized when the load is applied at the tip of a tooth. Therefore, the teeth are designed in such a way that when the contact point reaches a certain point at the tooth, the next pair of teeth starts to mesh as well. This divides the transferred load over multiple teeth and reduces peak stresses. This critical point is called the highest point of single tooth contact (HPSTC). Similarly, a point exist which is the lowest point of single tooth contact (LPSTC). The reduction of peak stresses leads to an increased fatigue life of the gear.

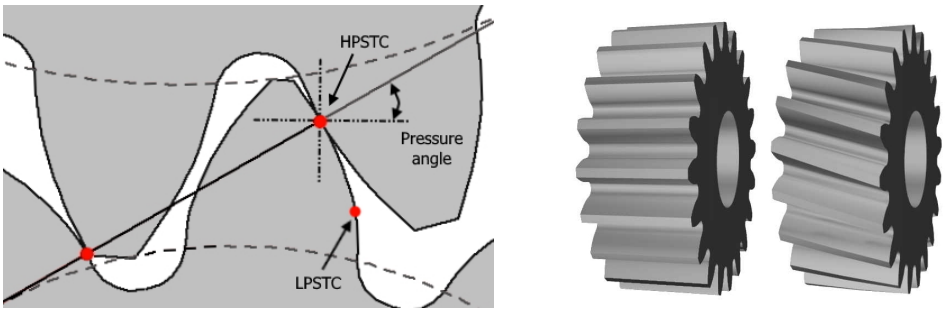

(a) (b)

Figure 2.1: (a) Schematic overview of two gears in contact showing the pressure angle and the contact points at HPSTC. (b) Examples of a spur and helical gear with straight and angled teeth, respectively.

Industrial gears can be roughly divided in two types: spur gears and helical gears. The difference is found in the angle of the teeth. The teeth of a spur gear are set along the parallel axis, whereas helical gears have teeth set at an angle (see Figure 2.1b). Helical gears are typically used in high-speed applications since they run smoother and make less noise. On the contrary, they bring in unwanted axial forces and are more complex to manufacture. Spur gears benefit from relatively low production costs due to its simplicity and are typically used for industrial purposes.

Material

Nowadays a large variety of materials are available on the market. In general this means that the optimal material properties can be selected for each application. In the case of gears, plastics and non-ferrous alloys are used in low power applications whereas steel alloys are the choice for more heavy duty power transmissions. As a result, the material choice is dependent of the processing characteristics such as machinability and hardenability, but also by the following performance characteristics:

- Bending strength: Bending strength is the amount of stress that can be applied on the tooth before plastic deformation occurs. A higher strength means more power can be transmitted by a single gear.
- Impact toughness: Industrial gears can undergo many impacts during its service time. These high force peaks can generate minor cracks each time they occur, directly reducing the life time of the a gear To counteract this effect and further crack propagation, sufficient impact toughness of the material is required.
- Bending fatigue strength: Due to cyclic mechanical loading in the root of the teeth, fatigue under bending can occur. To counteract the results of both low-cycle and high-cycle fatigue optimal material selection is of great importance.
- Wear resistance: High contact stresses and inadequate lubrication create micro-damage on and below the surface causing small pieces of material to break out of the tooth flank, this is called pitting. Another wear mechanism is scuffing, which is due to the combination of a rolling and sliding motion in the contact point creating abrasive wear at the flanks. Even at low contact stresses these phenomena occur. High wear resistance can be obtained by proper hardening of the contact areas of the tooth: the flanks.

Most medium and large-sized industrial gears are made from low alloy steels. Beside carbon, low alloy steel typically contains Cr, Ni and/or Mo particles, each contributing to performance improvement in their own way [9]. Nickel increases tensile strength, hardenability, fatigue strength and lowers critical temperatures for

heat treatment. For the latter this means lower temperatures and cooling rates can be applied during heat treatments. Chromium hardens the material, improving hardenability and wear resistance. Molybdenum, in combination with Chromium, contributes to the hardenability, but also increases the toughness of the material.

Various steel compositions can be produced. The final choice, however, is mostly depending on their availability. In western Europe, these alloys typically have carbon levels of 0.14-0.23% and Cr of 1.00-1.80%. Currently, the most commonly used gear steels are 20MnCr5 and 18CrNiMo7-6 [10]. The chemical composition of the materials are given in Table 2.1.

Table 2.1: Material compositions of the most commonly used gear steels 18CrNiMo7-6 and 20MnCr5.

Material	Fe	C	Cr	Mn	Si	Ni	Mo	S
18CrNiMo7-6	Balance	0.15-0.21	1.50-1.80	0.50-0.90	<0.40	1.40-1.70	0.25-0.35	<0.035
20MnCr5	Balance	0.17-0.22	1.00-1.30	1.10-1.40	<0.40	-	-	<0.035

2.1.2. Manufacturing

In order to determine the optimal way to repair gears and restore them into the original state, it is essential to fully understand the manufacturing process of gears. Gear production can be done by a large variety of processes. Gears with lower tolerances and applications involving minimal wear can be produced by processes such as extrusion or can be cut from a sheet material. Bigger gears, however, are far more complex to manufacture. Hence, more elaborate techniques are used. The process of gear manufacturing typically consists of 5 specific steps.

1. Manufacturing of the base cylinder: The base cylinder, often referred to as the blank, is the start of each gear. With large gears, a single block of base material is forged or cast into a cylinder whereas gears with a diameter up to 1000 mm are usually machined from a larger blank.
2. Tooth generation: The next step is roughly forming the teeth of the gear, gear cutting. This can be done in various ways but is mostly done by hobbing, shaping, broaching or milling. For industrial gears milling is usually the best option for the size of the gear.
3. Tooth refinement: When the rough shapes are formed, soft finishing is required to improve the accuracy and surface of the earlier prepared teeth. This is done by operations like shaving, grinding and lapping.
4. Heat treatment: To improve the material properties of the gears, a surface heat treatment called carburizing is performed. The main goal is to increase the wear resistance and fatigue life. At same time the process ensures the core material maintains its initial ductility and toughness since the heat treatment is only affecting the outer layer of the gear. A more detailed description about hardening will be given in the next paragraph.
5. Hard finishing: After the heat treatment is performed, a final finishing step is required to remove deviations such as small errors in the pitch and profile. This ensures that any wear, noise and other disadvantages are minimized or eliminated. Again, several options are available such as grinding, shaving and hobbing. In this stage typically only hundreds of millimeters are removed from the material.

Hardening

For a better understanding of the wear on tooth flanks, a full load cycle of the tooth is studied. At the beginning, the contact force consists of a combination of rolling and frictional sliding forces between the teeth (Figure 2.2a). When the contact point reaches the pitch line, sliding is gradually converted to pure rolling (Figure 2.2b), after which sliding occurs again, this time in the opposite direction (Figure 2.2c). The rolling movement induces so high local or so called Hertzian contact forces, which in some cases can lead to internal cracks and pitting. The combination of rolling with sliding introduces scuffing and abrasive wear. This wear on tooth flanks can be counteracted by increasing the hardness of the material. However, dynamic parts like industrial gears the aim is to obtain a tough core and a hard and wear resistant surface at the same time. To produce such a material property distribution, case hardening is typically applied.

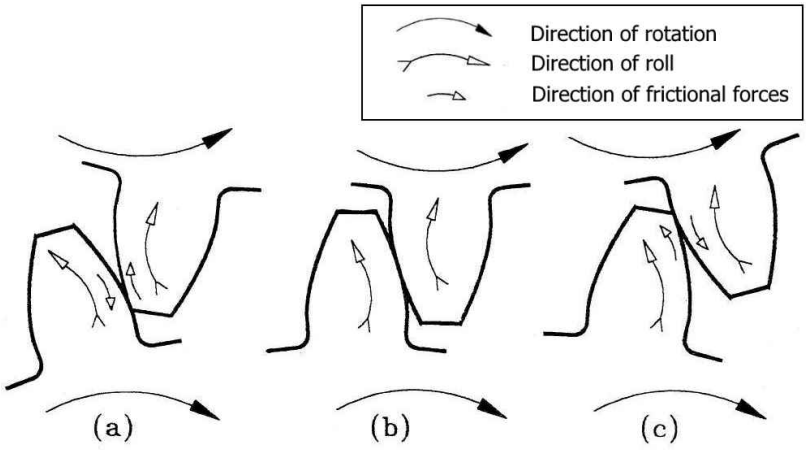

Figure 2.2: Kinematics of gear tooth contact forces at (a) the point of first contact (b), the pitch line and (c) final point of contact. Only at the pitch line, the contact forces consist of pure rolling. Reproduced from [11].

Case hardening can be done in multiple ways. In the context of manufacturing costs, processes which do not involve additive methods (welding or coating) or selective-hardening methods (flame, laser and electron beam hardening) are not suitable for industrial production purposes. Instead, less complex and cheaper methods such as diffusion hardening are used. Diffusion hardening is based on adding hardening elements such as carbon, nitrogen or boron to the surface of a heated substrate. With industrial gears mostly carbon particles are used [12], this process is called carburization.

The heat treatment process of case carburizing is a complex manufacturing step, requiring a high level of material and technical knowledge. However, its main advantage is its controllability. In the carburization process the substrate material is heated into the austenitic state to maximize the solubility for carbon present in the surrounding gas or plasma. The process is completed when the surface is quenched, transforming the austenite into the martensitic state. Several output parameters can be controlled to obtain the desired quality. The most important resulting output parameter for gears is the effective case depth, which is referred to as the depth where a hardness of 50 HRC or higher is measured. A basic formula for the acquired effective case depth follows from simple a diffusion consideration as:

$$x = \sqrt{Dt}, \tag{2.1}$$

where x is the case depth, D the diffusion coefficient and t the carburization time. The diffusion coefficient is depending on the carbon concentration around the part, substrate material and carburization temperature. The longer the steel is exposed to the carbon particles, the more diffusion will take place. Deeper cases need more time to establish. The desired thickness of the carburized case depends on the Hertzian forces that will be applied, which on its turn depend on the power the gear transfers. Usually this means, the larger the gear, the thicker the case. Typical effective case depths vary between 50 μm and 1.5 mm [12]. An example of a carburized gear tooth is shown in Figure 2.3.

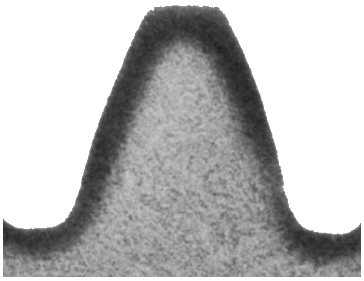

Figure 2.3: Section view of a carburized tooth showing the soft core material (light) and the carbon rich hard outer layer (dark).

Carburizing increases both the hardness and the fatigue strength of a material, which is very interesting for dynamically stressed components such as gears. Moreover, it creates a compressive stress in the outer layer of the material due to the quenching process, contributing to the hardness as well. However, the process is reversible and it should be noted that when a gear — and the carburized case in particular — is reheated, the diffusion process is continued. This means that the carbon present in the outer layer will start to spread further into the part. This process causes the gear to lose its desired material properties and compressive stress and reheating critical areas should therefore be minimized at all costs.

2.1.3. Failure

Under the extreme conditions in which industrial gears perform both the macro and micro-structure of the material are affected, eventually leading to malfunctioning. Gear damage is often related to errors or changes in the working conditions such as misalignment or high impacts. Most frequent damage is found at the teeth, where different types of damage can develop depending on the circumstances.

Multiple types of damage can be distinguished. Surface wear or micro pitting (Figure 2.4a and 2.4b) occurs due to the minor sliding movement of the teeth in combination with small abrasive parts. Although surface wear is inevitable, it should be minimized at all times. This can be done by correct alignment and good lubrication. Another type of surface damage is pitting. Pitting is initiated by micro-cracks at or below the surface and therefore harder to notice and more dangerous than abrasive wear. In an early stage, pitting can be repaired or confined, but when neglected it develops macro-cracks and leads to flank fracture (Figure 2.4c). The final common failure mode is due to material fatigue at the root. Many loads cycles weaken the material initiating micro-cracks. Often, a high impact such as a sudden stop of the mechanism can cause these cracks to propagate through the entire root, leading to tooth fracture (see Figure 2.4d). In the cases of root or flank fracture no proper repair solutions have emerged yet.

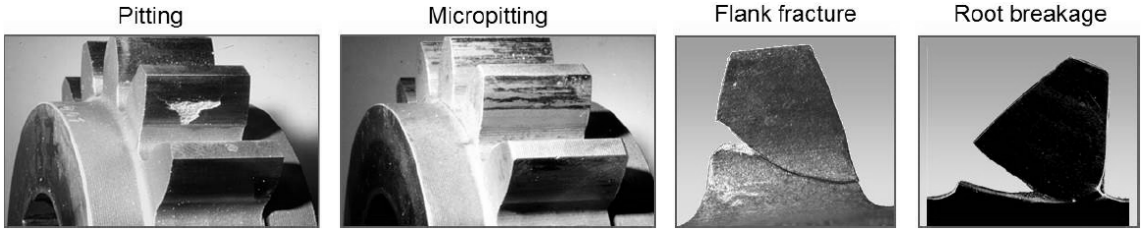

Figure 2.4: Different types of gear failure with surface damage (a, b) and catastrophic damage (c, d). Reproduced from [10]

2.2. Laser Metal Deposition

Additive Manufacturing is currently revolutionizing the manufacturing industry, with LMD as one of the most recently developed manufacturing techniques. Beside being applicable for part production processes, LMD is also very promising for the repair of damaged and worn out parts. Due to its relatively small heat input and uniform material deposition it is superior to conventional repair methods, leading to a new era where even end-of-life parts can be recycled. The next sections will elaborate on the history, the working principle and the characteristics of LMD.

2.2.1. History of LMD

The origin of LMD lies within the area of Additive Manufacturing and is based on layer-by-layer construction. In the late 1980's an increase of interest was seen in the field of stereolithography [13]. By pointing a guided UV laser beam on a layer of polymer powder, a certain pattern was melted and merged to the substrate after which a new layer of powder could be deposited. This process is called Selective Laser Sintering (SLS). When this process is repeated multiple times by stacking 2D layers, a polymer 3D structure was created. This was the very beginning of the now well-known 3D-printing.

Later, in the 1990's, the technology gained momentum and knowledge expanded rapidly. It also led to the development of commercially available polymer printers, the first 3D printers. Although this - polymer, layered structures - is the real root of 3D printing, the terminology seems easily interchangeable for other production processes within the area of AM nowadays. The products made with these 3D printers were mainly build from scratch and relatively quick to build. Moreover, costs dropped dramatically, making the technique extremely useful for Rapid Prototyping. Due to the fact that it is a computer aided and single step process barely any handling or human intervention is involved, limiting the amount of errors made. Another great benefit is the elimination of molds; small changes were easily made on the computer and products could be rebuilt quickly. It was no longer necessary to produce a new mold for every new prototype of a part. This significantly increased production speed.

In 1998, laser-engineered net shaping (LENS) was commercialized [14]. In the new production method, called direct laser deposition (DLD), laser or electron beams are used as a heat source. The choice of materials was no longer limited by polymers, since metallic materials became available. Another big change was the way of adding the material: instead of operating in a powder bed, the material to be deposited was now injected during the process. This could be done by feeding a wire or blowing powder. The latter form, however, is more commonly used since it's less sensitive to vibrations and provides a more accurate deposition [15]. Since the material was added only where it was actually needed, it led to a significant reduction of time and material.

From 2000 onward, more and more commercial systems were developed that could manufacture parts using different materials, including metals. Repairing and replacing parts became a lot easier and cheaper. Even tissue engineering with biomaterials are possible in the realms of AM. When multi-axis devices became available capable of making better, stronger and smoother depositions. Single piece products, 'parts in parts' and complex shapes were more easily produced using AM methods.

Latest developments in the area of LMD are research in hybrid laser manufacturing, a technique where multiple manufacturing steps are performed simultaneously. For instance, by adding of heat sources during a deposition in order to reduce thermal stresses in the deposited material. Another hybrid solution is be the implementation of both additive (deposition) and subtractive processes (turning or milling) into one system and in order a boost in efficiency. Other advantages of these hybrid laser manufacturing techniques are avoidance of material defects such as cracks, higher productivity, reduced residual stresses, cost reduction and improvement of processing times [16–18].

2.2.2. LMD Process

The LMD process is initiated by focusing a laser beam on a part or substrate. The local heat accumulation liquefies the material, creating a melt pool or molten pool. Powder is blown in this superheated droplet of metal through a coaxial nozzle using an inert carrier gas to prevent oxidation. Simultaneously, the laser head moves along the surface of the work piece leaving a track of solidified material. A schematic overview is illustrated in Figure 2.5. The laser follows a predetermined path and a layer of material is deposited on the work piece. Repeating this process multiple times will eventually create a multilayered, three-dimensional structure. After a short cooling period, the part is removed from the machine to undergo inspection for tolerances and cracks. Subsequently, the part is machined according to the desired dimensions.

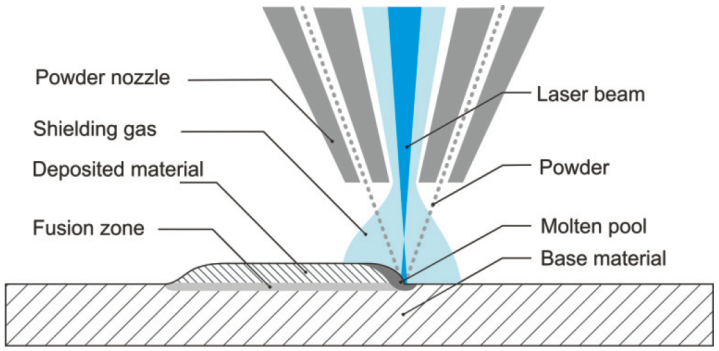

Figure 2.5: Schematic overview of the LMD process, showing the nozzle, substrate and the deposited material. The laser beam, powder flow and shield and shielding gas are focused at the melt pool. [19]

The main challenge in LMD is to create a track or layer with uniform properties throughout the deposited material. The properties of the deposition are determined by a great amount — at least 19 [20] — of parameters and machine settings, which should be tuned accordingly to obtain the optimal results. The primary process parameters for LMD are deposition rate, scanning speed and laser power. Figure 2.6 shows a schematic cross section of a track deposited on a substrate. The typical resulting output values for LMD are given in Table 2.2. They include the dimensions of the added deposited track, the extend of HAZ and the dilution. Dilution is defined as the ratio between the deposited material (red) and the mixed substrate material (orange) [21]. Mixing of the deposition material with the substrate can alter the resulting properties of the deposited structure when different materials are used. However, it is assumed that mixing are negligible for depositions with more than three layers. Other material properties such as density, porosity, microstructure and metallurgical bonding will determine the mechanical performance of the deposited material. Many studies have shown different results for the optimal parameter sets due to differences in the hardware of the setups such as nozzles and optical systems. Therefore a general setting for the LMD setup is not yet available.

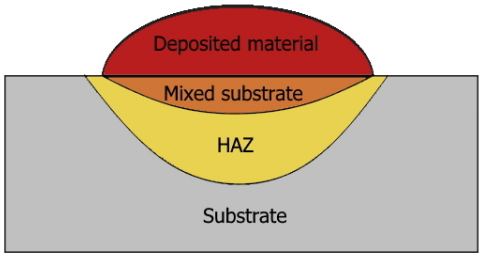

Figure 2.6: Cross section of a deposited track, showing the HAZ and mixing with the substrate and the resulting geometry. Reproduced from [21].

Table 2.2: Examples and common values of typical LMD output variables.

Variable	Value
Track width	0.5-3 mm
Track height	0.25-0.75 mm
HAZ	0.5-0.75 mm
Dilution	2-10%

2.2.3. LMD Setup

Various types of setups exist to different purposes of the machine. In general, the following 8 components can be distinguished in an LMD setup:

1. Guided arm: Depending on the movements and tracks that need to be deposited, the amount of Degrees of Freedom (DOF) can vary. In machines with planar operations, a 2 DOF (x-y) actuator could suffice whereas more complex projects demand more complicated systems such as fully mobile 6 DOF robot arms, similar to welding robots.

2. Stage: Every deposition starts on a substrate, which should be held in place during deposition. An either fixed or moving stage can be used for this, depending on the complexity of the geometry and demanded DOF. Typically, a rotating stage is used for the LMD process of round objects such as axles and gears, creating an extra DOF.

3. Laser source: The laser source is the most essential part in the setup. The laser power needed depends on the deposited material and the substrate. Although different laser types and power levels are used, CO_2 and Nd:YAG (neodymium-doped yttrium aluminium garnet) lasers with output powers up to 20 kW are usually preferred.[15, 22] The choice of laser type strongly depends on the aimed purpose of the machine.

4. Powder supply: Also called powder hopper. The material to be deposited is fed in powder form, often blown through plastic tubes by a carrier gas. In the powder supply, the powder is dropped on a spinning disc. The speed of the disc can be adjusted to control the powder flow rate. Since a constant material deposition is desired, the tube is kept as short as possible and the powder supply is typically located close to the robot.

5. Gas storage: The inert shielding gas is typically store in a tank or gas bottles. The pressure is held constant by a reduction valve. Like the powder, valve is located close to the process to make sure the gas flow rate is constant throughout the process.

6. Nozzle: A coaxial nozzle focuses the laser beam, the powder and the shielding gas at the desired location, as shown in Figure 2.5.
7. Protection: To protect both people and objects close to the setup from harmful gases and radiation, a screen-like construction is build around the setup. Usually this is in the form of a non transparent screen or cabin, combined with an air filtering installation.
8. Robot computer: The brain of the operation is a computer with customized software to control the process. It controls the powder supply, laser power, gas flow, and the movement of both the robot and the stage.

All mentioned components are depicted in Figure 2.7. The numbers correspond with the numbers in the picture.

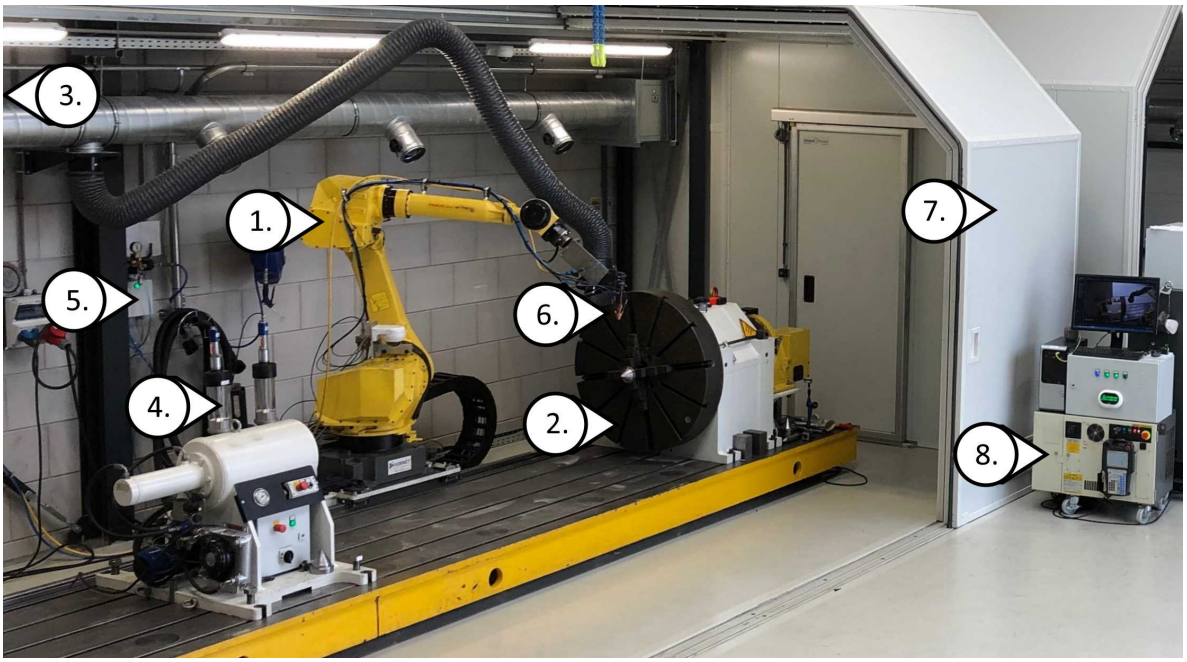

Figure 2.7: LMD setup and its components at GBS Gearbox Services. The laser source is not shown as it is located outside of the cabin.

2.3. Gear Tooth Analysis for LMD Repair

In general, when a part is repaired, it is key to understand its mechanical behavior. To make sure a repaired tooth is capable of withstanding the working conditions of the gear, a thorough analysis of a gear tooth is required. This analysis will serve as the basis for this research. During the lifetime of a gear the tooth undergoes multiple types of loading, introducing stresses in different areas of the tooth. These cycling loads bring in several failure mechanisms. The contact forces exist of both rolling and (minimal) sliding forces, whereas the root of the tooth encounters tensile and compressive stresses. Based on the different stresses during a load cycle, the tooth can roughly be divided in four areas of interest, all contributing to the performance of the gear. The properties of these areas, however, are extremely different. Ideally, with the flexibility of the LMD process it should be possible to match the preferences of every region without influencing others. The four areas (flank, core, root and interface) are depicted in Figure 2.8 and will be the basis of the problem approach in this research.

Tooth flank

The tooth flank is the outer layer of the tooth which makes contact with the meshing gear. It is typically case hardened and therefore harder — between 50 and 60 HRC — than the core. Higher hardness makes the

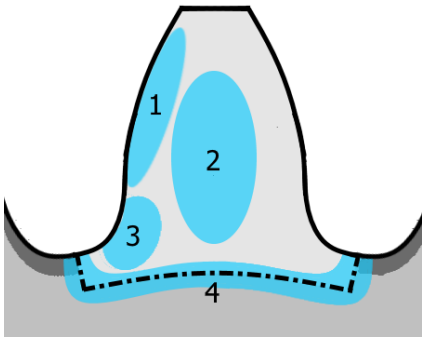

Figure 2.8: Different focus areas of a remanufactured tooth with the (1) flank, (2) core, (3) root and (4) interface. The carburized layer is illustrated with dark gray.

flanks of the tooth more resistant to wear and Hertzian contact forces. Study has shown that an increase in wear resistance can be achieved with the addition of a layer containing tungsten carbides and nickel super alloys [23]. Other attempts show promising results with respect to gear flank repair [24]. Worn off flanks of gear teeth have been replaced and successfully passed hardness tests. The main challenge of creating a wear resistant tooth flank is the creating a crack free deposition with sufficient hardness.

Core

The tooth core is described as the part of the tooth surrounded by the hardened case, with the fundamental function to withstand forces that reach through the hardened case. Typically, this core shows hardness values between 30 and 40 HRC [9], which will counteract crack propagation due to its ductility with small scale yielding. When only steels are considered, the flexibility of a tooth is barely influenced by the material choice. This can be deducted from the formula for the bending stiffness of a cantilever beam, which states:

$$k = \frac{3EI}{L^3}, \tag{2.2}$$

with,

$$I = \frac{1}{12wt^3}, \tag{2.3}$$

where k, L, w and t represent the bending stiffness, length, width and the thickness of a beam, respectively. It can be noted that the stiffness of a beam only depends on its geometry and Young's modulus. Since the geometry is known, this cannot be altered. In general, the Young's modulus of steel alloys varies between approximately 200 and 210 GPa and thus will not have a significant influence on the bending stiffness of a gear tooth. Furthermore, the core should be free of porosity and cracks. Any deviation in the core can contribute to crack initiation and premature failure.

Root

Of all areas in the tooth the root will undergo the highest stresses, caused by the normal force acting on the tooth. This results in compressive stresses on one side of the tooth, while on the other side tensile stresses are generated. Figure 2.9 shows the stress distribution when a tooth is loaded at the HPSTC. Tooth breakage in industrial gears is often originated in the root by the formation of small cracks. This crack initiation can have several reasons. Firstly, when an impact occurs by a abrupt stop of the mechanism for example. Due to the brittle hardened outer layer of the gear, this crack will quickly develop and propagate through the tooth, ultimately leading to failure. This phenomenon can be counteracted by selecting a tough material to reduce crack formation and propagation. The second failure mode is fatigue, which occurs when the root is subjected to excessive cyclic loading. The origin of fatigue strength is often blamed on wrong design or continuous overloading of the mechanisms. Cyclic stress concentrations at the root initiate cracks, eventually leading to root breakage. Typical values for the endurance limits of the root material are between 700 and 1050

MPa [9]. LMD offers the possibility to select a material that will contribute to the overall performance of the root.

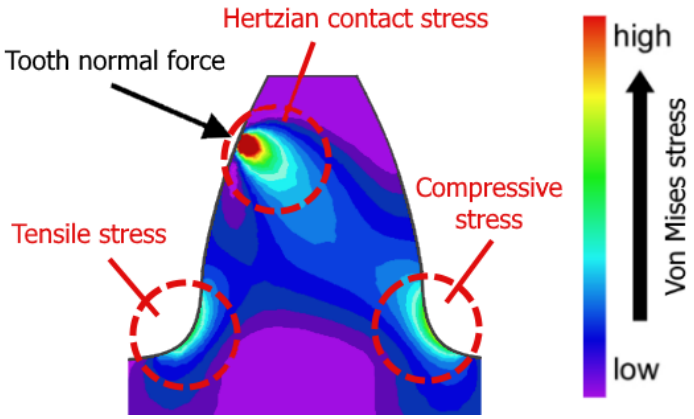

Figure 2.9: Schematic distribution of Von Mises stress inside a gear tooth induced by a normal force acting on the HPSTC. The highest stresses are located at the contact point and the tooth roots. Reproduced from [10].

Interface

Proper bonding between the new tooth and the gear is essential. The biggest problems are expected in the areas where material is deposited on the hardened layer. The presence of excessive carbon typically makes the dilution zone susceptible to the formation of highly brittle intermetallic phases. These phases are detrimental for the performance of the tooth due to the risk of crack formation. It has been found that with proper shape design, by using smooth corners and edges for instance, porosity can be avoided and the interface can greatly outperform the properties of the substrate [19, 25, 26].

2.3.1. Failure modes

As described in Chapter 1, gear failure is often caused by malfunctioning teeth with 2 types of damage in particular: tooth breakage and pitting. Moreover, LMD introduces new failure modes for all areas of a repaired tooth, as described in the previous paragraphs. The summary of the possible failure modes when using LMD for gear repair, as shown in Table 2.3, give and idea of the complexity of the problem. Where a chain is as strong as its weakest link, it is key to prevent any failure mode from occurring in order to make the best performing tooth.

Table 2.3: Possible failure modes after gear repair using LMD.

Location	Cause	Effect
Tooth flank	Low hardness	Abrasive wear
	Low case depth	Pitting
	Insufficient bonding	Flank detachment
Core	Porosity	Crack initiation
	Low Young's modulus	Lack of stiffness
	Low toughness	Crack propagation
Root	Low strength	Premature failure
	Fatigue	Crack initiation
	Low impact strength	Crack initiation
Interface	Intermetallic phases	Crack initiation
	Insufficient bonding	Tooth detachment

2.4. State of the Art: Gear Repair using LMD

The most common way to deal with broken parts or products is to remove the damaged area plus a bit extra and subsequently deposit new material to restore it. Since several deposition techniques came available over the past decades, it is of importance to choose the most suitable one for the specific repair purpose. Traditionally, gear repair was performed using fusion welding processes such as arc-welding or plasma welding. This did not lead to the desired result. Typically, it was seen that the abundance of heat input resulted in brittle teeth and a weakening effect in the surrounded material. With the rise of LMD, new possibilities have emerged. Laser aided manufacturing, and LMD in particular, seems to be an outstanding process compared to conventional repair processes such as arc welding or coating technologies.

Due to the use of guided arms and computer based manufacturing the process is, and the heat input in particular, highly controllable. It is known that the thermal history plays a dominant role in the quality of AM structures. In conventional methods, such as welding, the abundance of heat is often accompanied by detrimental effects such as weakening of the substrate and extreme thermal stresses in the deposited material. Low heat exposure and depth of the laser ensure minimal thermal distortion in the surrounding material. In other words, the HAZ remains relatively small compared to other manufacturing techniques [24]. Furthermore, a superior metallurgical bonding between the substrate and the added layer can be created due to the controllable and typically low dilution. A low dilution can be favorable in cases where sharp transitions in material properties are required or when mixing of the substrate material is detrimental for the deposited material. Another great benefit of LMD is minimized porosity due to the controllable environment. The overall performance properties of the depositions are excellent and the bonding usually is stronger than welding techniques or processes where the material is sprayed on, such as thermal spraying. All the above properties of the LMD result in more homogeneous microstructures [21, 27].

More advanced techniques are becoming available nowadays. This leads to more ways to use LMD as a repair technique. Currently, a lot of research is done for the build up of 3D structures. Functionally graded materials can have great benefits under certain circumstances, such a the ductile core combined with the hard and wear resistant outer surface of a gear tooth. It is demonstrated that such structures can be created, albeit with a complicated production process [28, 29]. Another achievement is the increase in efficiency it is a time-consuming process to determine the geometry of an old part, whereas drawings are not always available. Therefore, new ways are yet to be implemented. By combining sensors and computer programs researchers are now able to apply reverse engineering for the restoration of worn-out or damaged parts [30], leading to a radical drop in production time while at the same time giving more accurate results.

In conclusion, it can be said that with the extreme flexibility of the LMD process it is not a question of 'if' but 'how' we can use LMD to repair a broken gear.

3

Research Approach

The main goal of this research is to replace a gear tooth using LMD with a performance similar to that of an original carburized spur gear. The combination of the complex material composition, the high demands regarding the mechanical properties of gears and the difficulties that are found in LMD makes this goal a big challenge. This study describes an empirical research on a relatively new topic and hence a straight forward procedure does not exist. To come to a substantiated solution within the limited time and budget the research approach is not based on exploring one specific step of the repair process of a gear. Instead, it is working towards a comparison between a deposited multilayer structure and traditionally manufactured tooth. It should give insight on the feasibility and pitfalls of using LMD as a repair technique for tooth breakage of gears. This chapter describes the general repair approach, the methodology and the used testing procedure in this research.

3.1. General Idea

The problem initiating this research is tooth breakage of a carburized 18CrNiMo7-6 spur gear. The goal is to find a solution to repair such a broken tooth in preferably the simplest and fastest way. Using the knowledge presented in Section 2.3, a multi-step repair plan for gears with tooth breakage is formed.

1. Tooth breakage has caused a gear to malfunction. The dimensions are determined for the remanufacturing process.

2. LMD needs a smooth and clean surface to make sure the bonding between the old and new material is as strong as possible. This is done by milling away the remaining material of the broken tooth.

3. A core material, with mechanical properties comparable to the core of an 18CrNiMo7-6 gear, is deposited roughly in the shape of a tooth. This will later be the core and root of the replaced tooth. The basic shape of a tooth is milled out, including some extra material from the flanks.

4. A hard, wear resistant layer is deposited on the flanks of the structure. The tooth is then completed by grinding or milling the hard layer into the involute profile of the gear. The gear is now ready for use.

The four distinct steps are illustrated in Figure 3.1. It can be noted that the remanufactured tooth will consist of two different materials, whereas a gear is made from a single material and case hardened. The reason for this choice is that a deposition material that is both sufficiently tough for the root and wear resistant for the flanks in the as-deposited state does not exist. A deposited tooth made from a single material would need an additional hardening process to obtain the required mechanical properties of the remanufactured tooth. These hardening processes typically involve a lot of heat input in the gear. As discussed in Section 2.1.2, this is not favorable in the case of hardened gear, since the additional heat is detrimental for the remaining carburized layer and performance of the repaired gear.

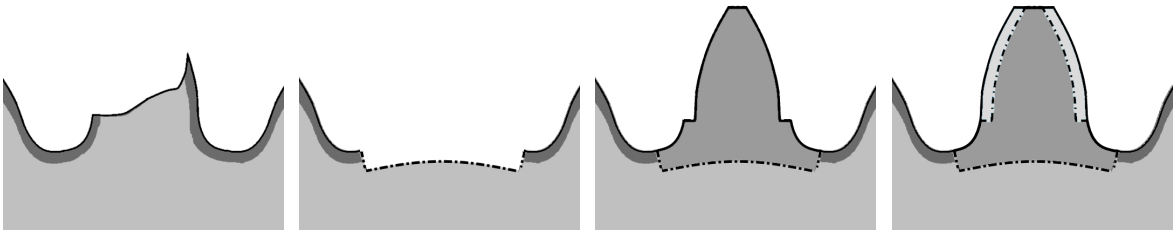

Figure 3.1: The four steps of the repair cycle of a tooth with (a) the broken tooth, (b) tooth removal, (c) core material deposition and (d) flank material deposition. The carburized layer is illustrated with dark gray.

3.2. Interface Dimensions

In preparation of a repair process, the excess material is removed. To minimize the risk of tooth detachment in service conditions, the interface is intentionally located away from high stress concentrations that are present at the root. In order to do this, the tooth is milled away at the centerline between two adjacent teeth up to the point where the material that is not affected by carburizing is reached. The depth of the milled groove is approximately 2 mm (twice the hardened case depth). This way the dilution zone with the hardened surface material is as small as possible and the majority of newly deposited material can bond to the material of the gear that is not affected by carburizing. Moreover, the interface is located perpendicular to the hardened layer to avoid any shear forces in this critical area. The solution is illustrated in Figure 3.2.

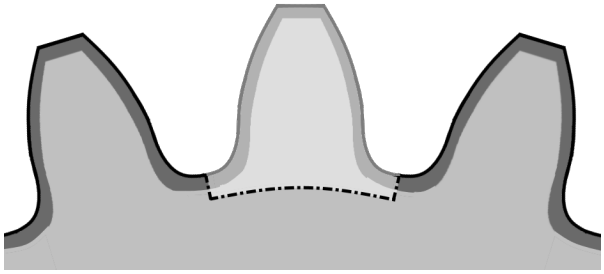

Figure 3.2: Schematic image of the tooth removal before deposition. The removed part is indicated with the dotted line. The groove ends at the centerline between 2 adjacent teeth, perpendicular to the carburized layer (dark gray).

3.3. Parameter Selection

With the large amount of different setups used in literature, it is impossible to come up with general set of deposition parameters for the repair of gears. Since the LMD process is dependant on a numerous amount of deposition parameters only the most dominant parameters are considered in this research. First of all, not all parameters can easily be changed. This includes parameters such as gravity and powder temperature. Others are proven to barely influence the process outcome and therefore are based on in-house experience. Examples of fixed parameters in this research are carrier gas flow rate and laser beam diameter. The selected parameters for this research are the primary process parameters (powder mass flow, laser power and scanning speed), two types of material and other factors that may influence the process of building a 3D structure. The latter includes the scanning pattern, interpass temperature, preheating and post heating. An overview of the investigated parameters and the chosen values is given in Table 3.1.

3.4. Test Plan

This research is focused on finding a relatively quick way generating a tooth-like shape with mechanical properties comparable to a case hardened gear tooth. Based on the material properties of a tooth and the foreseen

Table 3.1: Overview of the investigated deposition.

Parameter	Values
Material	Inconel 625, Inconel 718
Deposition rate	0.20, 0.25 g/s
Scanning speed	900, 1000, 1100 mm/min
Laser power	1700, 1900 W
Deposition pattern	Parallel, Crosswise
Preheat temperature	20, 120, 220°C
Interface geometry	Square, Round
Interpass temperature	80, 100, 130°C

failure modes shown in Table 2.3, a structured multi-step test plan was constructed. In general, the research consists of two main parts, each covering three steps. The first part is aimed at investigating the influences of several deposition parameters on the mechanical properties of the core material. In the second part, a custom test setup is used to test for influences of the thermal cycle on the plastic and elastic deformation of deposited tooth shaped structures. The empirical multi-step test plan is structured such that each step is generating data and knowledge for the next one. The aim is to work towards a final set of deposition parameters for the repair process of industrial gears. Typically, in a scientific report the complete methodology is presented before the results. However, in this report a total of six steps, all using several testing methods, are described. To keep the report structured and readable it is chosen to only present a general description in this section. A more detailed description and the motivation for the selection of the tests used in each step will be given in Chapter 4, prior to the corresponding results.

3.4.1. Part 1: Core Material Properties

Following the approach shown in Section 3.1, it can be seen that the larger part of the repaired carburized gear tooth is made of core material. Since the core material is used at the core, root and interface, it should be tested elaborately on multiple types of mechanical properties. The first part of the tests in this study aim to find a suitable set of deposition parameters for this core material, using different standard testing methods. The goal is to obtain a core material with mechanical properties similar to bulk 18CrNiMo7-6. This is done in the three steps shown below.

1. Material selection and primary process parameters: This initial step is aimed on finding the best settings in order to deposit a crack free and homogeneous core material. This is done by comparing different materials and the primary deposition parameters: laser power, scanning speed and deposition rate.

2. Interface with the gear: The bonding to the case hardened layer of a gear is expected to play a crucial role since the formation of carbon concentrations often leads to crack initiation. By altering the shape of the interface, the preheating temperature of the substrate and the effective heat input during deposition, differences in bonding quality are tested.

3. Multilayer structures: To manufacture a new tooth on a broken gear, a multilayer structure must be deposited. In this step, the influence on the mechanical properties of built up multilayer blocks is investigated by changing the scanning pattern and preheating temperature.

3.4.2. Part 2: Mechanical Behavior

The second part of the study focuses on differences in mechanical behavior of tooth-shaped structures. Using a special developed test setup, it is focused on improving the mechanical properties of the deposited structure in order to work towards a comparison with a traditionally manufactured tooth. This is done in three steps.

1. Interpass temperature: Thermal history plays a dominant role in the quality of deposited structures. By adjusting the interpass temperature the cooling rates can be controlled, affecting the resulting microstructure of the deposited material. Interpass temperature is defined as the maximum allowed temperature of the deposited structure at which a subsequent layer can be initiated.

2. Hard flank: A hard flank layer should be added to the deposited tooth structure to increase its wear resistance and to make it comparable to a carburized tooth. The deposition of this hard layer involves reheating of the previously deposited core material, likely changing its microstructure and mechanical properties. This step investigates the effect of the deposition of a hard flank on the performance of the core structure. Note that no further investigation is done on the improvement of the mechanical properties of the deposited flank layer.
3. Final comparison: The final part of this research consists of a comparison between a traditionally produced reference tooth and a deposited tooth using LMD. The results should clarify whether the used approach is suitable for the repair of gears.

3.5. Laser Setup

The experiments done in this study are carried out with the setup depicted in Figure 2.7. It uses a 6-DOF FANUC-M710ic50 robot arm equipped with a 4000 W LDF diode laser. The spot size is fixed at 4 mm with a focal distance of 12 mm. An additional rotational stage is installed, but not used in this research. Powder is supplied by a MAN 41000 DE 06 powder hopper. A gas with 99,9998% Argon is functioning as both a shielding and carrier gas and is focused into the laser beam at the coaxial nozzle.

3.6. Material Testing

In this research physical testing is performed to determine several material properties. Technical guidelines and specifications for destructive and non-destructive testing of metals are provided by many standards. Typically, the guidelines of the International Organization for Standardization (ISO) are followed in European countries. However, since LMD is such a newly applied technique in the industrial world, there are no official standards for multilayer LMD process. Hence, it is considered as an overlay welding process. ISO standards are followed when possible. To be capable of withstanding the working conditions of a gear, the different areas of a tooth require different mechanical properties. This calls for multiple types of testing. The tests that are used in this research are listed below.

- Dye penetrant testing: Dye penetrant testing is used to detect discontinuities at the surface of the material. First, the surface is cleaned and sprayed with a colorant and left for 20 minutes to let it soak into surface defects by capillary action. After removal of the excess colorant, a white spray called the developer is applied. The developer draws out the colorant from cavities and cracks. The change in color marks the location of defects at the surface. The process is depicted in Figure 3.3.

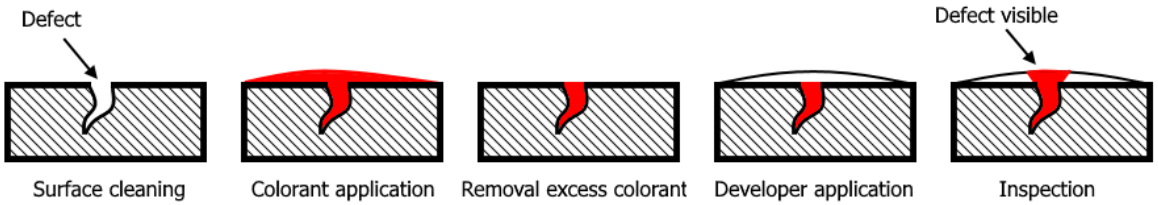

Figure 3.3: Picture of an indent made through an optical microscope. The green lines are automatically drawn by the software and are used to determine the dimensions of the indent.

- Macroscopic testing: In preparation to macroscopic testing, the surface of interest is ground and colored using cleaning vinegar as an etchant. A picture is taken with a USB camera. Subsequently, the 'IC Measure' software package is used to measure the dilution and layer height of the deposition. The test gives insight on the shape of the interface, the HAZ, dilution and geometry of the deposited material.
- Microscopic testing: Microscopic testing is use to reveal the macro and microstructure of a material. It gives insight in the presence of micro-cracks and impurities. The specimen is cut and the surface of interest is polished and etched. Subsequently, the surfaces are captured through an optical microscope using different magnifications. The microscopic tests in this research are performed at the metallurgical laboratory of the MME group.

- Side bend testing: In a side bending test, 10 mm thick specimens, consisting of a substrate material with three layers of deposited material on top, are bent around a steel cylinder with a diameter of 40 mm using a hydraulic cylinder. By bending the specimen to an angle of 180°, large stresses and deformation are induced in the deposited material, leading to cracks or rupture in some cases. A specimen passes a test when no signs of cracks show up during visual inspection. A side bend test gives insight on the bonding quality (between layer and different materials), soundness and ductility of the deposited material. A picture of the bending setup is shown in Figure 3.4. The choice for side bending tests are based in the standard testing procedure for overlay welding [32].
- Face bend testing: Face bend testing is similar to side bend testing, but the direction of bending is perpendicular. In face bend test the deposited material is on the convex side of the specimen, maximizing the applied strain in the deposited material. Face bend testing typically shows a lower pass rate than side bend testing. A test is considered as 'passed' when no cracks are visible.

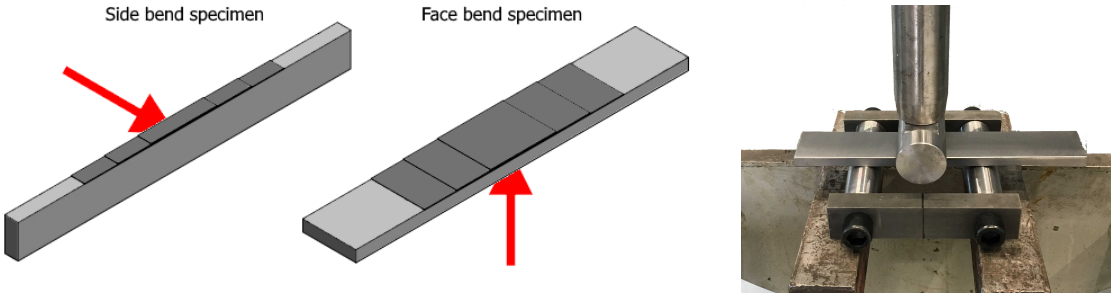

(a) (b)

Figure 3.4: (a) sketch of the side and face bending samples showing the direction of loading in the bending test. (b) picture of the bending setup including a sample before bend testing.

- Tensile testing: In a tensile test a specimen is clamped at two ends and slowly pulled apart until the material fails, while stress and strain are measured. A tensile test gives insight in the the Young's modulus, ultimate tensile strength, yield strength and elongation of the tested material. Figure 3.5 illustrates the dimensions in mm of the used tensile test specimen in this research.

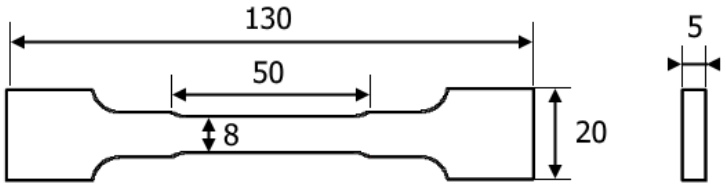

Figure 3.5: Schematic drawing of the tensile test sample, including dimensions in mm.

- Charpy impact testing: In a Charpy impact test, also known as Charpy V-notch test, a pendulum with a predefined weight is dropped onto a specimen with a notch. The amount of energy that is absorbed by the sample during fracture is a measure of the material's impact toughness. It also whether the sample material has a ductile or brittle fracture mechanism. Figure **??**a shows the dimensions of the samples used in this research.

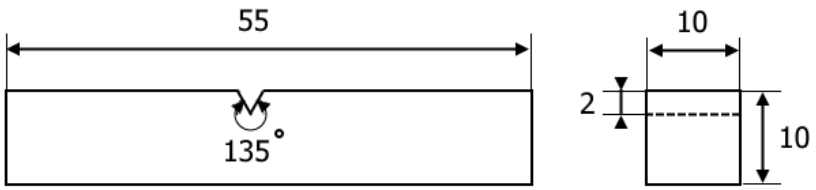

Figure 3.6: Schematic drawing of the Charpy impact test sample, including dimensions in mm.

- Hardness testing: In a hardness test an indent is made with a pyramidal diamond indenter. A known constant force of 1 to 100 kgf is applied for 10 to 15 seconds. Using a microscope the size of the indent is measured, as shown in Figure 3.7a. Subsequently, the hardness can be deducted from the dimensions of the indent. The used test in this research is the HV0.5 test converted to HRC values using the ISO hardness conversion table [31].

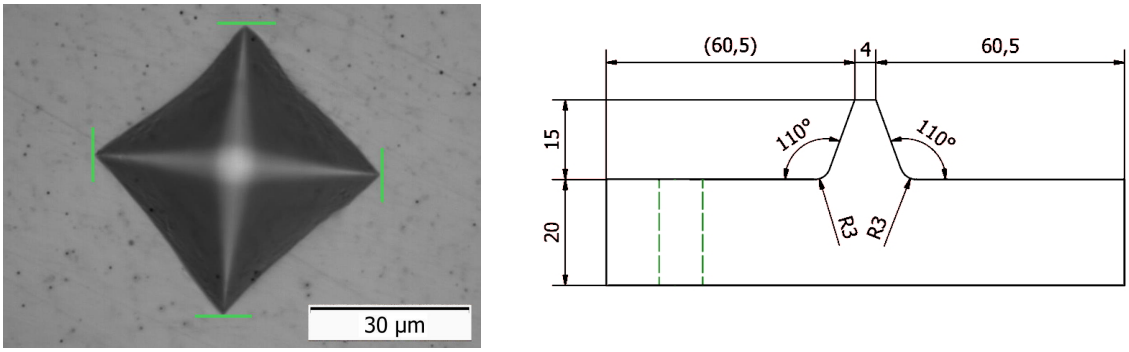

(a) (b)

Figure 3.7: (a) Picture of an indent in Inconel 718 from the optical microscope. The green lines, automatically drawn by the software, are used to determine the dimensions of the indent. (b) Schematic drawing of the single tooth rack test specimen including the dimensions in mm.

- Static load testing: A specially designed test setup applies a slowly increasing force on a single tooth rack specimen until failure occurs. The setup is designed such that a pressure angle of 20° can be applied at the HPSTC. The test gives insight in the plastic and elastic behavior of a tooth-shaped test specimen as shown in Figure 3.7b. It also shows the failure mechanism of a broken tooth. The selected force rate in this research is 625 N/s. A more detailed description of the setup is found in Appendix A.

3.6.1. Substrate material

To obtain the most reliable and repeatable results it is favorable to standardize the tests where possible. The selected gear material is 18CrNiMo7-6, one of the most common materials for hardened gears. All depositions use substrates which are cut from the same certified piece of bulk 18CrNiMo7-6 steel. Initial depositions are performed on circular slabs with a diameter of 320 mm and a thickness of 20 mm, as shown in Figure 3.8a. The size of the substrate allows the deposition of large surface and serves as a heat sink when multilayer structures are deposited. Depositions involving smaller dimensions of the deposited structures generate a lower total heat input and therefore require less heat dissipation. A smaller substrate is used with a size of 200 × 125 × 20 mm, as can be seen in Figure 3.8b. Note that these smaller substrates are case hardened and milled to mimic the interface of a carburized gear with a milled out tooth.

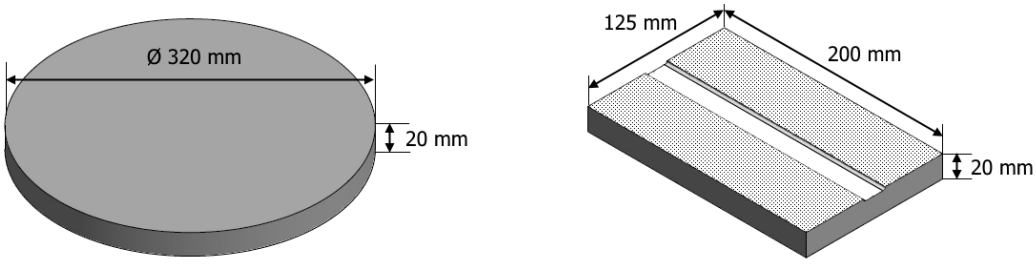

(a) (b)

Figure 3.8: Schematic view of the 18CrNiMo7-6 substrates with the corresponding dimensions. (a) substrate for large depositions and (b) carburized substrate with a milled groove for smaller tests.

4

Results and Discussion

The backbone of this research is the basic multi step testing plan presented in Section 3.4. Due to the amount of tests it is chosen to combine a more detailed explanation of the tests and their corresponding results into this single chapter. The results from each step will serve as input for subsequent steps, building up towards a final comparison between an deposited and a traditionally manufactured tooth.

4.1. Part 1: Core Material Properties

This first part aims on finding a suitable set of deposition parameters of the core material in order to create a core with the desired mechanical properties. Since this is related to the core, the root and the interface of a repaired tooth, this will be the larger part of this research. First, the material choice and basic deposition parameters are investigated. After that, more focus is put on the bonding quality and the mechanical properties of a deposited 3D structure.

4.1.1. Material Selection and Primary Parameters

The initial step is aimed on finding the best settings in order to deposit a crack free and homogeneous core material. This is done by comparing different materials and the primary deposition parameters: laser power, scanning speed and deposition rate.

The first challenge is to find a core material with mechanical properties comparable to the iron-based 18CrNiMo7-6 gear steel. However, iron based powders in general have a lower fatigue strength and are less available due to oxidation risks. Therefore, the selected deposition materials to be chosen for this research are Inconel 625 and Inconel 718, both nickel based superalloys. Even though both materials are usually heat treated to increase their strength, these materials are known for their weldability and ductility in the as-deposited state as well. Another characteristic feature of the selected materials is the heat resistance, which could contribute to the stability of the microstructure when reheated. This should reduce weakening effects due to short-term high heat exposure when for instance the flank material is deposited. Furthermore, it is known that a nickel based filler material is a stabilizing element for laser welding carburized low alloy steel, increasing the bonding strength and reducing risks at high carbon concentrations [33]. The mechanical properties and chemical compositions are shown in Table 4.1 and 4.2 respectively.

Table 4.1: Mechanical properties of 18CrNiMo7-6, Inconel 625 and Inconel 718 bulk material.

Material	Young's modulus (GPa)	Yield strength (MPa)	Ultimate tensile strength (MPa)	Elongation (%)	Impact toughness at 20°C (J)
18CrNiMo7-6	210	700	1000-1250	>8	>30
Inconel 625	208	414-758	827-1103	>30	>66
Inconel 718	204	1030	1280	>12	>40

Table 4.2: Chemical composition of the gear steel and the selected powders according to the suppliers.

Material	Ni	Cr	Fe	Mo	Nb	C	Mn	Si	Ti	Al
18CrNiMo7-6	1.40-1.70	1.50-1.80	Balance	0.25-0.35	-	0.15-0.21	0.50-0.90	<0.40	-	-
Inconel 625	Balance	21	<5	9	4	-	-	-	0.4	0.4
Inconel 718	Balance	18	18	3	5	-	-	-	1	0.6

In addition to the material selection, the influence of the scanning speed, deposition rate and laser power on material properties are investigated. Selected parameters are based on the in-house experience of single layer depositions of the selected materials. All parameters and their values are found in Table 4.3, the remaining parameters are kept constant. Combining all parameters will lead to 2^4 samples. By applying the orthogonal Taguchi test vector, the amount of deposition parameter combinations is reduced from 16 to 8 in total, as shown in Table 4.4. In this design of experiments a vector is chosen in a way that the response between parameters is uncorrelated while minimizing the amount of tests.

Table 4.3: Parameter overview for testing the primary process parameters of the core material.

	Parameter	Value 1	Value 2
A.	Material	Inconel 625	Inconel 718
B.	Scanning speed	900 mm/min	1100 mm/min
C.	Deposition rate	12 g/min	15 g/min
D.	Laser power	1700 W	1900 W

Table 4.4: The applied parameters combinations for testing the primary process parameters of the core material using the corresponding parameters and values from Table 4.3.

	Parameter			
Deposition no.	A.	B.	C.	D.
1	1	1	1	1
2	1	1	2	2
3	1	2	1	2
4	1	2	2	1
5	2	1	1	1
6	2	1	2	2
7	2	2	1	2
8	2	2	2	1

The substrates for the depositions in these tests are ⌀320 × 20 mm 18CrNiMo7-6 steel plates. On top of the plates, 3 layers of material are deposited, decreasing in size to create a stepped structure as shown in Figure 4.1a. After the 8 depositions, each sample is cut into 5 specimens: 2 strips of 40 mm wide for face bend testing and 3 strips of 10 mm for 2 side bend tests and macroscopic examination, illustrated in Figure 4.1b and c. The test procedures in this part are based on the standards for overlay welding [34] and mainly include tests to quickly evaluate the influence of the parameters and distinguish major differences.

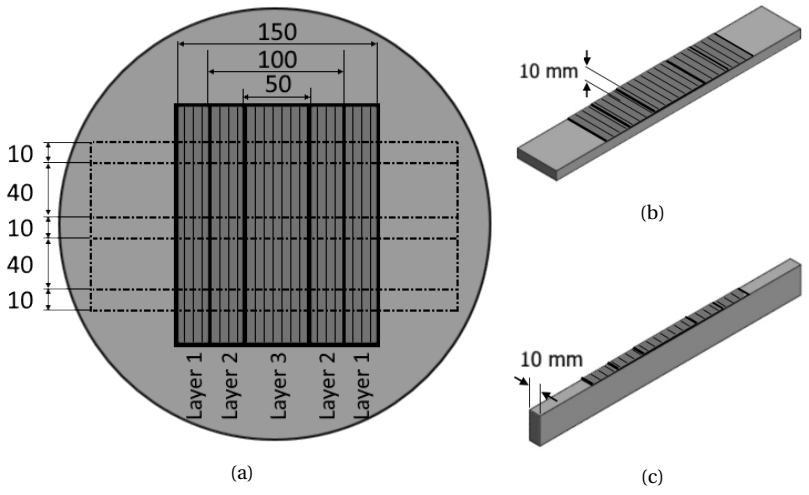

Figure 4.1: (a) Schematic overview of the round substrate and 3 deposited layers, including the deposited tracks, cutting lines (dotted) and dimensions in mm. The resulting (b) face bend and (c) side bend and macroscopic examination samples.

Macroscopic testing reveals the interface and layer quality of the depositions. Figure 4.2 shows an example of the cross section of a single layer of Inconel 718 deposited on a 18CrNiMo7-6 substrate. All samples show a similar constant and wavy interface with no visible signs of porosity. This typically implies a sound bonding with the substrate as a results of a good set of deposition parameters. According to this observation it is assumed that the chosen parameters do not have a significant effect on the bonding quality.

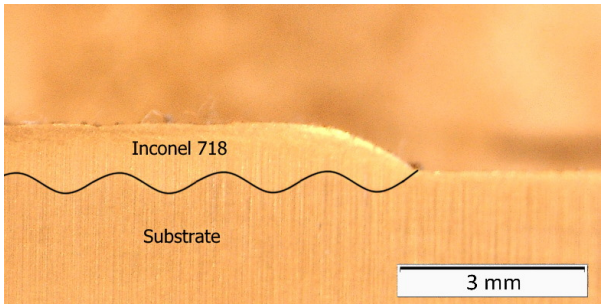

Figure 4.2: Cross section of a single layer of Inconel 718 on a 18CrNiMo7-6 substrate showing the constant and wavy interface.

Figure 4.3 shows the side bend specimens after testing. All test specimens have passed the side bend test considering no cracks or defects are visible with the unaided eye. This proves for good soundness and ductility of the deposited materials. Additionally, it is concluded that a proper bonding is achieved in all parameter combinations.

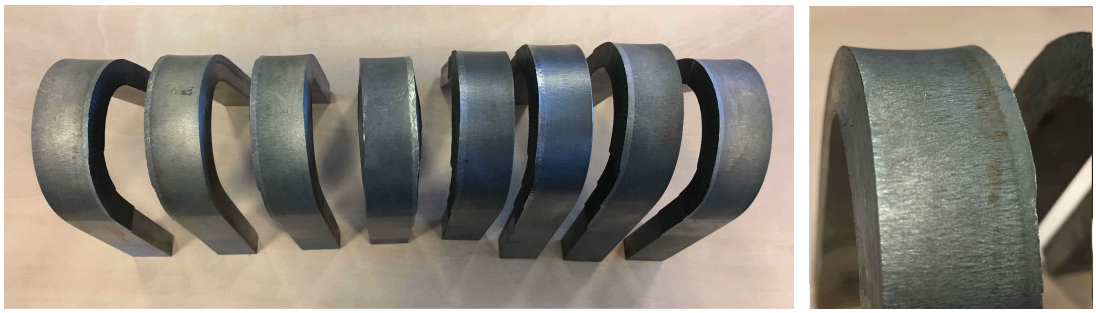

(a) (b)

Figure 4.3: (a) One side bending test specimen from each of all combinations after testing. All tests passed since no signs of cracks are visible. (b) A close up of the area of interest with the largest deformation.

The results for the face bending test are shown in Table 4.5. As expected (see Section 3.6), the pass rate is lower than the outcome of the side bending tests. It can be noted that only 6 out of 16 specimens have successfully passed the face bending test. A difference is found in the choice of material, a significant improvement of Inconel 718 over Inconel 625 is seen. This shows that a better soundness for the deposited Inconel 718 is achieved with the selected primary process parameters. From Table 4.1 it is seen that bulk Inconel 625 tends to have superior ductility and fracture toughness compared to bulk Inconel 718. Looking at the presented results, it can be concluded that these mechanical properties of Inconel 625 cannot be matched with current deposition parameters.

Table 4.5: Results face bending test for different parameters.

Parameter 1	No. of tests passed	Parameter 2	No. of tests passed
Inconel 625	1/16	Inconel 718	5/16
1700 W	5/16	1900 W	1/16
0.20 g/s	1/16	0.25 g/s	5/16
900 mm/min	3/16	1100 mm/min	3/16

Furthermore, a difference in outcome is noted using different deposition rates and laser power. Test with the higher deposition rate and lower laser power show better results. A lower deposition rate or higher laser

power result in a higher amount of energy input into the substrate increasing the dilution. In this case, more substrate material is mixed into the deposited material, causing it to level out the mechanical properties of the deposited material. However, this phenomenon is only present in the first few layers and therefore less relevant for this research. The parameters for further research, based on the outcome of the tests above, are given in Table 4.6.

Table 4.6: Deposition parameters for the core material used for further research.

Parameter	Value
Material	Inconel 718
Laser power	1700 W
Scanning speed	1000 mm/min
Deposition rate	0.25 g/s

4.1.2. Interface with Gear

The bonding strength between the gear and the deposited tooth is determined by the quality of the interface. Any contamination or stress concentrations within the deposited material could lead to crack initiation and should thus be avoided. This is obtained by a continuous, smooth interface, without sharp corners. Effects on the smoothness of the interface is studied by comparing different groove shapes. Typically, a square groove is the most simple and therefore cheapest way of milling a groove. However, since the powder is deposited vertically onto the substrate it is expected that a sharp corner of the groove could lead to porosity and sharp corners in the interface. For comparison, a round groove shape is tested as well. The geometries of both groove shapes are shown in Figure 4.4.

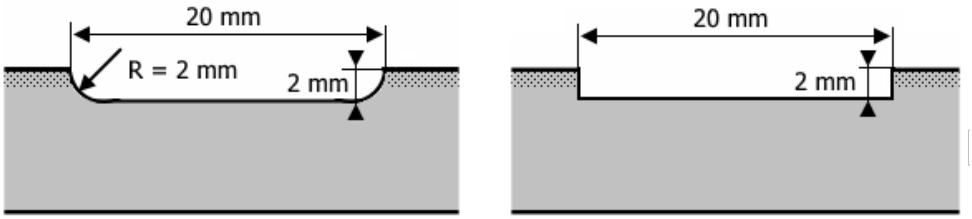

Figure 4.4: Detailed cross section of the milled groove shapes in the case hardened substrates. The hardened layer is represented by the dotted areas.

Furthermore, the interface between the deposited material and the case hardened layer of a gear is investigated. It is known that the elevated concentration of carbon in the hardened layer can cause the formation of carbides. These brittle intermetallic particles significantly increase the chances of fracture. Similar effects are observed when welding hardened steels. Here the solution is found in altering the thermal history. This suppresses the carbon diffusion and prevents the formation of high carbon concentrations. This effect is studied by changing the preheat temperature of the substrate and using different effective heat inputs. However, the HAZ should be kept as small as possible to avoid any changes in the gear material. The effective heat input is defined as the ratio of laser power to the scanning speed and can therefore be altered by adjusted one of them. It is chosen to change the scanning speed, since this did not have a significant effect on the results of the previous tests, shown in Table 4.5. An overview of the three tested parameters influencing the quality of the interface is given in Table 4.7. All parameters are combined, leading to a total of 2^3 depositions.

Table 4.7: Deposition parameter overview to investigate the quality of the interface between the deposited material and the case hardened substrate.

Parameter	Value 1	Value 2
Groove shape	Round	Square
Scanning speed	800 mm/min	1200 mm/min
Preheat temperature	20°C	220°C

All 8 depositions start with a 200 × 125 × 20 mm 18CrNiMo7-6 substrate. The blocks are case hardened and a 20 mm wide groove is milled out according to the desired shape using a CNC milling machine. Subsequently, when the substrates are cleaned and the grooves are partly filled with the deposition of Inconel 718 (Figure 4.5a). The remaining deposition parameters are shown in Table 4.6.

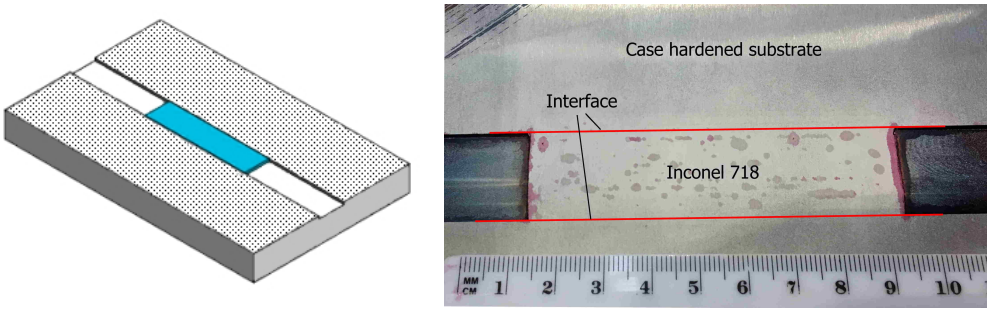

(a) (b)

Figure 4.5: (a) Schematic view of the substrate showing the partly filled groove (blue) and the carburized layer (dotted). (b) Top surface of the dye penetrant tested sample showing impurities like cracks and cavities (red dots). Contamination is present in the deposited material, but not on the interface with the case hardened layer.

When the samples are cooled to room temperature the top surface is ground and dye penetrant tested to expose any cracks or impurities at the interface. From dye penetrant testing in Figure 4.5b it is seen that no impurities or cracks are present at the interface between the Inconel and the case hardened layer of the substrate. Instead, contamination was seen in the Inconel 718. Further investigation should point out the reason for this unexpected result.

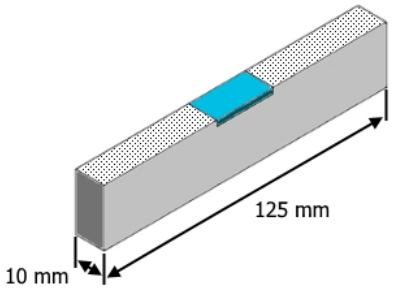

Figure 4.6: The cut test specimen for macroscopic and hardness testing showing Inconel 718 (blue) and the carburized layer (dotted).

A 10 mm wide slice is cut out, as shown in Figure 4.6. Macroscopic testing is performed on the cross section to study the interface and HAZ. All cross sections of the samples show a constant and wavy interface. Figure 4.7 shows a comparison of the outcome for different groove shapes. It is found that the HAZ and dilution in both cases is quite similar. However, the interface of samples with a round groove shape appear to be slightly smoother, whereas the samples with a square groove show sharper edges. Non-smooth transitions are often accompanied by local stress concentrations. A round groove shape is thus preferred for further research.

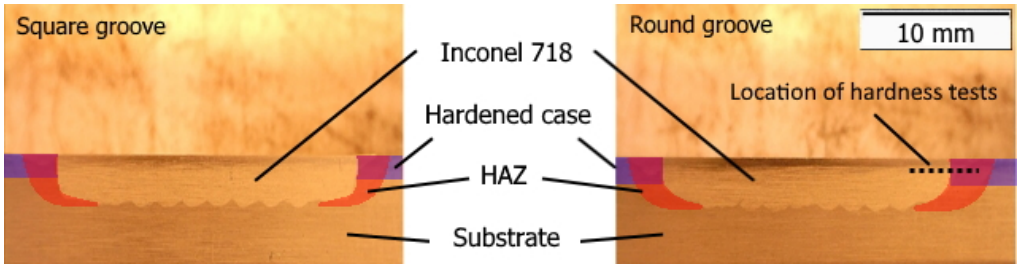

Figure 4.7: Cross section of a square (left) and round (right) groove filled with Inconel 718, showing the hardened case, resulting HAZ and the location of the hardness test.

To check the interface between the gear and the deposited tooth for unwanted intermetallic phases a HV0.5 hardness test is performed. The samples are polished and tested with 10 indentations in a straight line spaced 0.3 mm apart. The line starts at the deposited Inconel 718 and ends in the case hardened layer of the substrate, as depicted in Figure 4.7. The results of the hardness measurements are shown in Figure 4.8a. No peaks or local concentrations of hardness were observed for any of the samples, indicating the absence of unwanted intermetallic particles such as carbides. Even indentations at the sharp interface of Inconel 718 and the substrate (Figure 4.8b) do not show hardness peaks. When this result is combined with the absence of cracks and impurities at the interface, it is assumed that formation of detrimental carbides is counteracted by the stabilizing effect of the nickel present in the Inconel 718.

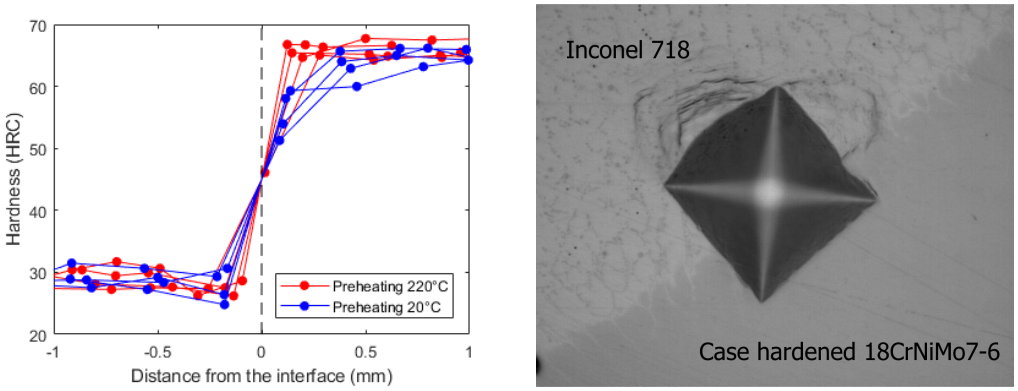

(a) (b)

Figure 4.8: Hardness measurements around the interface between Inconel 718 and the case hardened 18CrNiMo7-6 substrate with (a) resulting hardness as a function of the distance from the interface for different parameter settings and (b) an image of the indentation at the interface.

Regarding the hardness profiles for different process parameters, no significant differences are seen for altering groove shapes and heat inputs. Figure 4.8a shows the hardness profiles for different preheat temperatures. A less sharp hardness profile is observed for higher preheat temperatures. As mentioned in Chapter 2, the carburization process of the 18CrNiMo7-6 steel induces compressive stresses at the surface, contributing to the material hardness. The elevated initial temperature at the higher preheat temperature of the substrate leads to a larger area of stress relaxation, creating a less steep hardness profile. The steeper hardness profile is not considered detrimental for the quality of the bonding, since the interface with the carburized layer is located away from high tensile stresses.

In this step, the bonding quality of deposited Inconel 718 on a case hardened 18CrNiMo7-6 substrate was investigated. It is found that the geometry mainly influences the shape and smoothness of the interface. Neither the change in heat input nor the preheat temperature showed a significant effect on the quality of the bonding. No signs of thermal cracking or indications of unwanted particles at and around the hardened case were found. It is therefore expected that the interface will not play a dominant role in the performance of a remanufactured tooth. Nonetheless, impurities were found in the Inconel 718. The next section will elaborate on the performance of a structure built using LMD and shows the possible detrimental effects of the found contamination. The parameters for further research are given in Table 4.8.

Table 4.8: Process parameters regarding the interface between the gear and deposited tooth used for further research.

Parameter	Value
Groove shape	Round
Scanning speed	1000 mm/min
Preheating	20°C

4.1.3. Multilayer Structures

In order to manufacture a new tooth on a broken gear, a multilayer structure must be deposited. The influence on the mechanical properties of a built up multilayer structure is investigated by changing the scanning pattern and preheat temperature. This is followed by destructive material testing to study the differences in mechanical behavior.

The mechanical performance of a deposited multilayer Inconel 718 structure is mainly influenced by the thermal history and the resulting grain structure. In multilayer nickel based powder depositions it is not uncommon to observe the formation of detrimental columnar grains. These grains are formed during the solidification of the molten powder. The properties of these grains are highly dependent on the scanning direction and are typically oriented in the direction of deposition. It is shown that a more equiaxed structure shows better isotropic properties [35, 36]. To achieve such a microstructure, sharp orientation changes from one layer to another are required. This creates a more homogeneous structure and contributes to an increase in ductility. Therefore, the first investigated parameter in this step is the build-up pattern. The two patterns considered are parallel and crosswise deposition. Figure 4.9 shows the schematic overview of the two patterns. Both patterns use a zigzag track with a 50% track overlap. In the parallel pattern, each layer is deposited with the same scanning pattern. The crosswise deposition uses a 90° rotation between each layer.

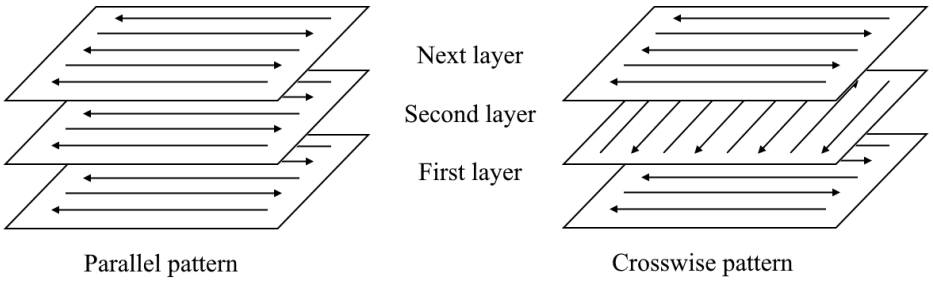

Figure 4.9: Different scanning patterns to used to examine effects on the mechanical properties of multilayer structures.

Due to the rapid heating and cooling cycles during LMD, often detrimental thermal residual tensile stresses are built up in the deposited material. Preheating is known to reduce these thermal stress due to a smaller temperature difference between the substrate and the recently deposited material. To investigate the effect of preheating on the mechanical properties of a deposited structures multiple preheat temperatures are used. However, this research is focused on repairing a carburized gear. This means that the temperature of the gear should not exceed the tempering temperature (approximately 300°C) for long periods of time as it is detrimental for the properties of the carburized layer. The considered preheat temperatures are 0°C, 120°C and 220°C.

Table 4.9: Parameter overview for the deposition of multilayer structures. All values are combined, leading to 6 combinations.

Parameter	Value 1	Value 2	Value 3
Pattern	Parallel	Crosswise	
Preheat temperature	0°C	120°C	220°C

Combining the parameter values from Table 4.9 leads to a total of 6 depositions. Remaining parameters are shown in Table 4.6. For each test a large substrate (⌀ 320 × 20 mm) is cut and cleaned to avoid any contamination during deposition. A structure of Inconel 718 is deposited on top with a total size of 140 × 45 × 25 mm, as illustrated in Figure 4.10a. After deposition, the structures are removed from the substrates. From each block a total of 4 test specimens is extracted using wire EDM: 2 samples for both a tensile test and a Charpy impact test, as shown in Figure 4.10b. It is chosen to extract the samples perpendicular to the deposition direction, in case any anisotropy occurs due to the formation of columnar grains. This way, these grains are oriented perpendicular to the loading direction and typically shows the worse results than other loading directions in terms of the strength and elongation of the deposited material. An example of the resulting deposited structures and tensile samples are shown in Figure 4.11a and 4.11b, respectively.

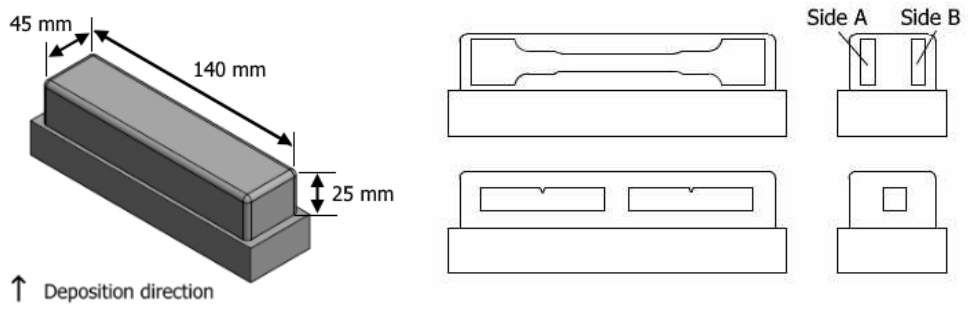

(a) (b)

Figure 4.10: (a) Schematic overview of the deposited structure and (b) the locations of extraction for the different tensile test and Charpy v-notch samples.

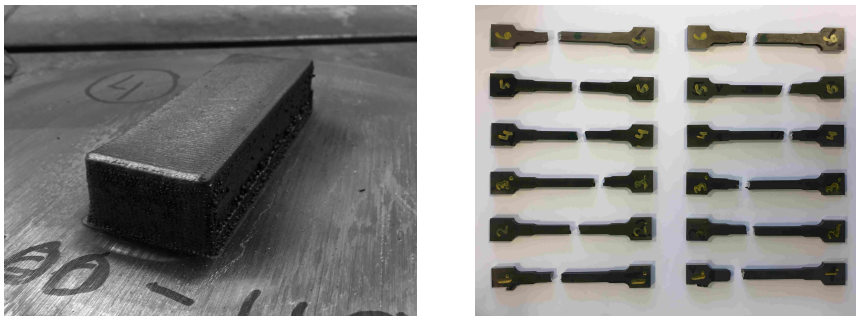

(a) (b)

Figure 4.11: (a) Deposited multilayer structure of Inconel 718 using a crosswise deposition and (b) the tensile test specimens after testing.

Figure 4.12 shows the tensile test and Charpy impact test results for different scanning patterns. An increase for almost all resulting variables is achieved when a crosswise deposition is used. However, it is known that for a homogeneous material the elongation and ultimate tensile strength of a material are inversely related. This means when the ultimate tensile strength is increased, the elongation at break is decreased. Since this does not hold for the shown results, it indicates that parallel deposition results in a less homogeneous microstructure As expected, strong influence of the scanning pattern is seen. This is attributed to the orientation change between subsequent layers, reducing the formation of columnar grains. When comparing the mechanical properties of the deposited core material with the desired properties — for 18CrNiMo7-6 gears, shown in Table 4.1 — several things can be noted. Firstly, it is seen that a crosswise deposition of Inconel 718 leads to a superior impact strength. The resulting structure also show a comparable elongation at break. However, the Young's modulus, yield strength and ultimate tensile strength do not have the desired outcome and will need further investigation.

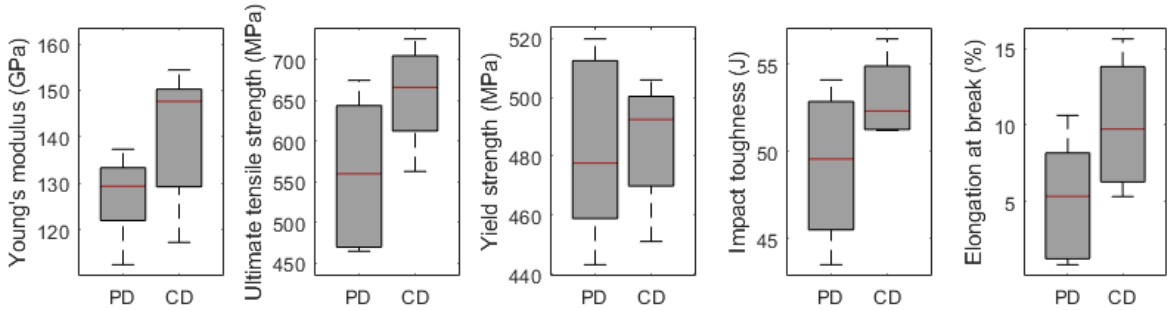

Figure 4.12: Tensile test results showing median and standard deviation for Parallel Deposition (PD) and Crosswise Deposition (CD) of Inconel 718 structures. Each box represents a total of 6 tests. The central mark indicates the median, and the bottom and top edges of the box indicate the 25th and 75th percentiles, respectively.

Figure 4.13 shows the tensile test and Charpy impact test results for different preheat temperatures. It is seen that there is no significant effect on the mechanical properties of deposited Inconel 718 structures due to preheating of the substrate. The absence of this effect is attributed to the heat accumulation during the multilayer build up of the structure. Especially in the top part of the deposition the lack of heat dissipation is much smaller, causing the interpass temperature to rise and make the preheat temperature negligible. This makes preheating relevant for only the first few layers of a deposition. A better parameter to control the heat cycle of each layer is the interpass temperature, which will be done in a later part of this research.

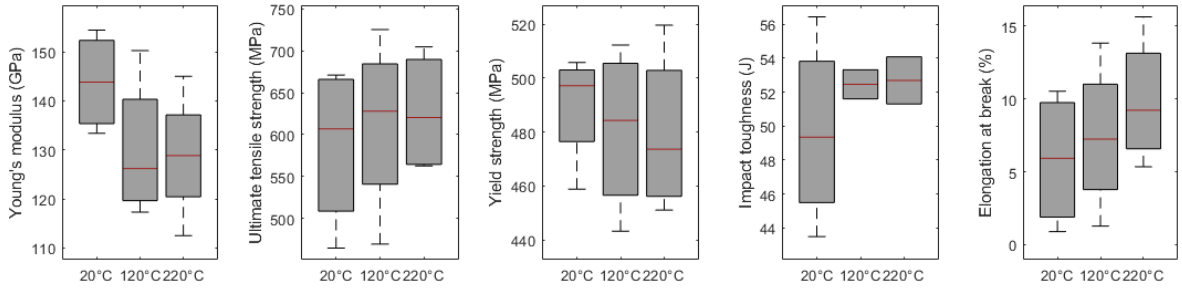

Figure 4.13: Tensile test results showing median and standard deviation for different preheat temperatures of Inconel 718 structures. Each box represents a total of 6 tests. The central mark indicates the median, and the bottom and top edges of the box indicate the 25th and 75th percentiles, respectively.

Another aspect that stands out from Figure 4.13 is the large deviation in the measurements. This raises questions about the quality and repeatability of the deposition. Looking at the fracture surfaces in Figure 4.14 of both the tensile test specimens and the Charpy impact test specimens, a lamellar pattern of disc-shape defects are observed. This indicates a partly ductile and brittle fracture within the independent deposited tracks and layers. This type of inhomogeneity can often be led back to impurities such as oxides formed during the deposition process. These impurities are specifically found on the outside of a single track and are known for the contribution to a more brittle fracture mechanism of the deposited material.

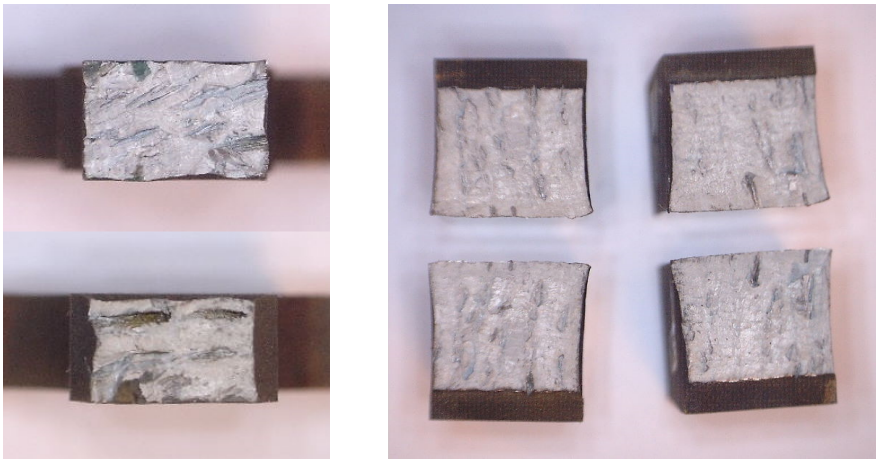

(a) (b)

Figure 4.14: Fracture surfaces of a (a) tensile test specimen and (b) Charpy impact test specimen built in a crosswise pattern, without preheating. Disc shape defects can be noted.

Besides large deviation the results show a very low and inconsistent Young's Modulus. As mentioned in 3, the Young's modulus is expected to be between 200 and 210 GPa for all steel alloys. Since the geometry and testing circumstances are considered equal, an explanation for the reduced elasticity is found in Hooke's law, which is described as:

$$E = \frac{\sigma}{\epsilon}, \tag{4.1}$$

with

$$\sigma = \frac{F}{A}, \tag{4.2}$$

where E, ϵ, F and A represent the the Young's modulus, elongation, applied force and the effective surface, respectively. Assuming that the measurements of the tensile tester are calibrated, the only variable affecting the elastic modulus is the effective surface. When the effective surface is reduced, for instance by internal cracks or cavities, actual stresses in the test specimen are much higher than calculated and can thus drastically reduce the resulting mechanical properties. The measured average Young's modulus of the samples is approximately 65% of the expected value. This would imply that the effective surface should be reduced with 35%. However, another explanation for the low Young's modulus is found in the following equation:

$$G = \frac{E}{2(1+\nu)}, \tag{4.3}$$

where G, E and ν represent the bulk modulus, Young's modulus and Poisson's ratio, respectively. Since the bulk modulus is assumed to be constant for steels, it can be deducted that a reduction of Poisson's ratio leads to a lower Young's modulus. Poisson's ratio describes the ratio of tensile elongation and the corresponding perpendicular compression due to tensile loading of a material. A reduction of Poisson's ratio can be achieved by the presence of disc-shaped defects, causing for a local decoupling of the perpendicular stresses in the material. It is therefore assumed that the disc-shaped defects shown in Figure 4.14 are the main cause for the low Young's modulus and strength.

Further investigation on the results show a dependency on the location of extraction of the specimens from the built up block structure. A clear example of the effect on the ultimate tensile strength is presented in Figure 4.15b. Combined with the poor mechanical properties and party brittle fracture mechanism, these large differences are attributed to a lack of shielding gas during the depositions. Insufficient shielding gas used during deposition is allowing the continuous formation of unwanted impurities such as oxides. These particles float on the melt pool and solidify in the outer layer of a track. In a subsequent track they are partly remelted and picked up by the melt pool, causing an gradually increasing amount of contamination throughout a layer. Figure 4.15a shows the distribution of contamination across a deposited layer. This principle also holds for multiple subsequent layers, leaving a highly uneven distribution of impurities in the structure. Due to this mechanism, the contamination is located at one side of the structure with parallel deposition since it uses unidirectional scanning. Crosswise deposition, on the contrary, is less affected whereas impurities are distributed over two sides due to the 90 degrees orientation change between each layer, as can be seen in Figure 4.15b.

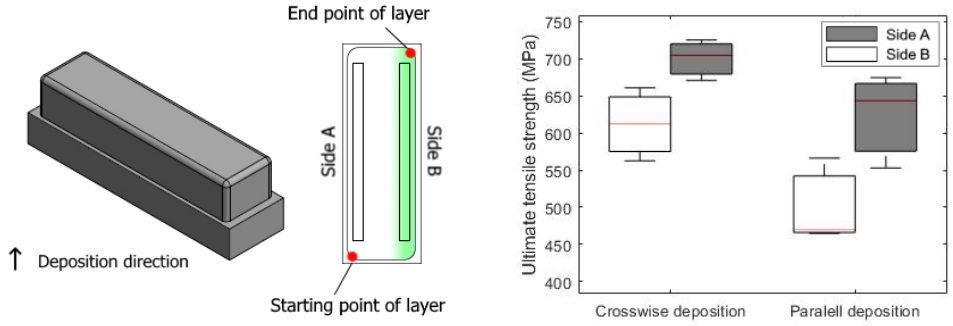

(a) (b)

Figure 4.15: (a) Schematic drawing of the built up contamination (showed in green) throughout a deposited layer. (b) Ultimate tensile strength for different locations of specimen extraction and different deposition patterns. Each box represents a total of 3 tests. The central mark indicates the median, and the bottom and top edges of the box indicate the 25th and 75th percentiles, respectively.

Additional testing: Shielding Gas Flow Rate

It was found that the previous depositions most likely have suffered from a lack of shielding gas. To exclude effects of impurities additional testing is performed with an adjusted shielding gas rate. New tensile specimens are built with a crosswise deposition pattern without preheating and the same parameters from Table 4.6 . The shielding gas flow rate is increased from 10 l/min to 20 l/min. Since the impact toughness has proven to be satisfactory, no Charpy impact test is done.

The results in Figure 4.16 show an improvement in mechanical properties with the adjusted shielding gas. The Young's modulus was significantly increased to a satisfying 208 GPa. The ultimate tensile strength and yield strength also slightly improved, whereas a drop in elongation at break was observed.

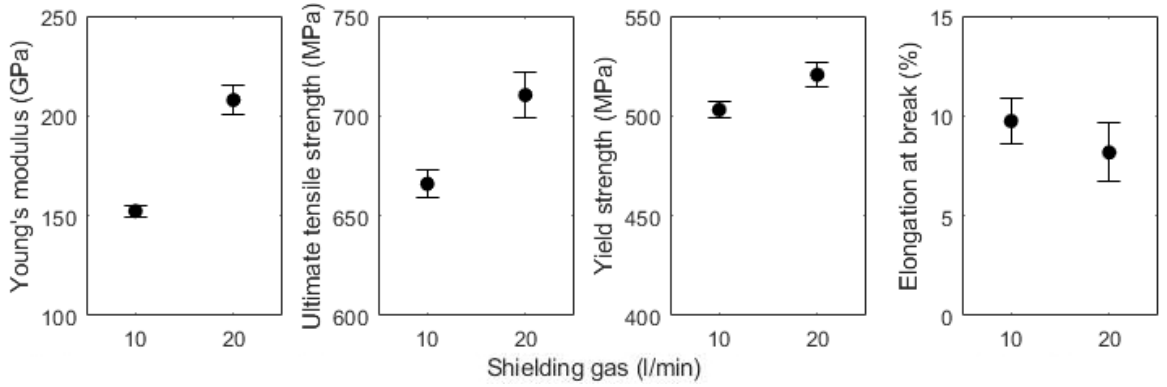

Figure 4.16: Averages and standard deviations of the mechanical properties for depositions with different shielding gas flow rates, using a crosswise deposition and no preheating. Each point represents a total of 3 tests.

The fracture surface is shown in Figure 4.17a. A less brittle fracture is observed with less distinctively visible tracks compared to the results shown in Figure 4.14. Nonetheless, minor lamellar fracture surfaces are present. The outer surface of the specimen shows a periodic waviness, as can be seen in Figure 4.17b. Measurements show an approximate peak to peak spacing of 1.7 mm, correlating with the distance between 2 adjacent tracks in a layer. This appearance is created by local deformations, indicating weaker and stronger parts within each track. It is therefore concluded that the periodic inhomogeneity is not caused by a lack of shielding gas and should be investigated further.

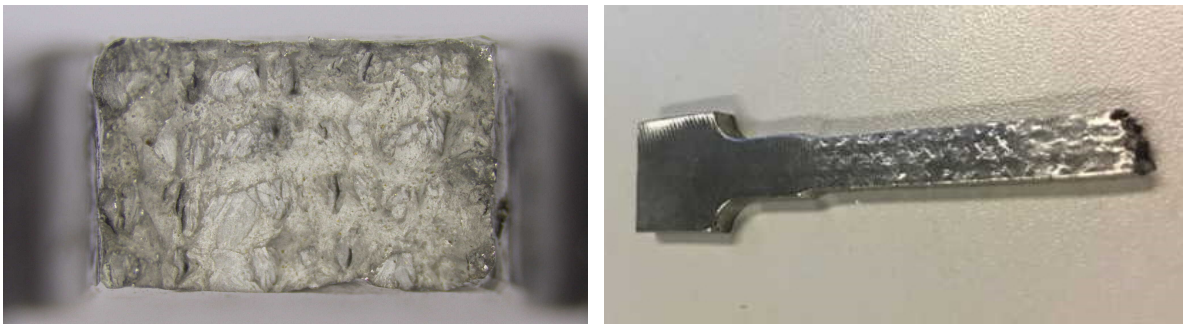

(a) (b)

Figure 4.17: (a) Fracture surface and outer surface (b) of a tensile specimen built with the adjusted shielding gas flow rate of 20 l/min.

Microscopic testing is performed to expose the inhomogeneity and possible contamination within the tensile test specimens. After polishing and etching, the specimens are investigated and photographed through the optical microscope. The results of the metallurgical examination are shown in Figure 4.18a-d. As can be seen in Figure 4.18a, the shown cross sections originate from the part of the sample that was not loaded during tensile testing. This means that the remaining images depict the results of the as-deposited material. Figure 4.18b clearly shows the separate tracks and layers including dilution zones and slight differences in grain size. The material contains multiple cracks which are initiated during or right after the deposition process. Moreover, no impurities or contamination is observed within the material or the cracks. These observations

combined with the lamellar fracture surfaces show that the presented cracks are caused by liquation cracking. Furthermore, it is seen that the deposited structure shows a highly dendritic microstructure. Figure 4.18c shows the transverse section whereas in Figure 4.18d the cross sections of the dendrites are visible. These dendrites have a detrimental effects on the mechanical behavior of the deposited structure. A reduction of both liquation cracking and the formation of a dendritic microstructure can be achieved by changing the thermal cycle of the deposited material.

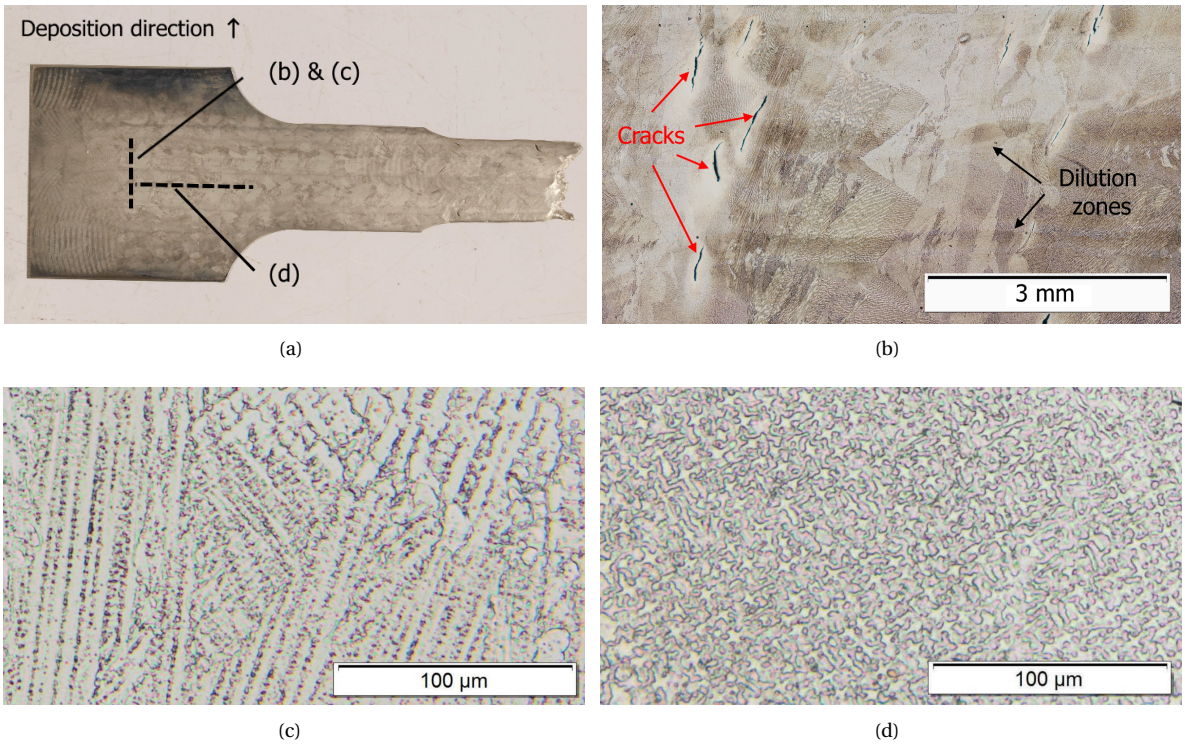

(a) (b)

(c) (d)

Figure 4.18: Different cross sections of a specimen built with adjusted shielding gas flow rate. (a) The specimen and the locations of microscopic examination. (b) Transverse section at 50x magnification, showing liquation cracking and the dilution zones. (c, d) Transverse and longitudinal section showing the columnar dendrites at 200x magnification.

A comparison of the resulting mechanical properties of the deposited Inconel 718 structure and bulk 18CrNiMo7-6 gear steel is given in Table 4.10. It is seen that both the Young's modulus and the elongation are similar. Furthermore, it is noted that the yield strength and ultimate tensile strength of the deposited material are approximately 70% of the desired values. Based on the findings in the previous paragraph, it is expected that further testing on the thermal cycle of the deposition will reduce this difference in mechanical properties.

Table 4.10: Resulting mechanical properties of multilayer depositions and bulk 18CrNiMo7-6. Deposition parameters: shielding gas flow rate of 20 l/min, crosswise deposition pattern and no preheating.

Material	Young's modulus (GPa)	Yield strength (MPa)	Ultimate tensile strength (MPa)	Elongation (%)	Impact toughness at 20°C (J)
As-deposited Inconel 718	208 ± 5.2	521 ± 4.5	710 ± 8.3	8.2 ± 1.03	>50
18CrNiMo7-6	210	700	1000	8	>30

4.2. Part 2: Mechanical Behavior

This final section of the research is working towards a comparison of the plastic and elastic behavior of a deposited and a case hardened tooth. This is done in three steps. The first two steps aim at defining the influences of the thermal history on the performance of the deposited structures. The reviewed parameters are the interpass temperature and the addition of a hard flank layer using LMD. The last step of this part — and this research — includes the comparison of the static mechanical behavior of a deposited structure, including hard flanks, and a case hardened 18CrNiMo7-6 tooth. The remaining deposition parameters for the core material are based on the previous tests and can be seen in Table 4.11.

Table 4.11: Deposition parameters for the core material of the tooth shaped specimens.

Parameter	Value
Material	Inconel 718
Laser power	1700 W
Scanning speed	1000 mm/min
Deposition rate	0.25 g/s
Groove shape	Round
Preheat temperature	20°C
Deposition pattern	Crosswise
Shielding gas flow rate	20 l/min

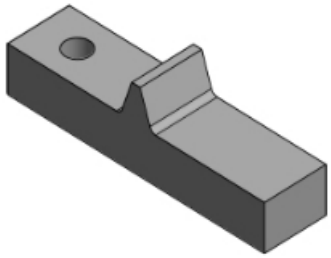

Figure 4.19: Single tooth rack test specimen used in the this part of the research.

Since the effects of the studied parameters in the first two steps are based on the thermal history, they are highly geometry dependant. Therefore, regular mechanical testing can no longer be used. Instead, a specially designed setup is used to measure the performances of a deposited tooth-like shapes. All tests in this part of the research are performed on this setup, using a single tooth-rack test specimen as shown in 4.19. A full description of the setup and the test specimen is found in Appendix A.

The used substrates for deposition are case hardened 200 × 125 × 20 mm 18CrNiMo7-6 steel blocks. After hardening, the substrates are milled to create a round groove with a width and depth of 20 and 2 mm, respectively. The specimens are produced by depositing an oversized tooth structure of 120 mm long. Subsequently, the long structures are milled into the tooth shape (Figure 3.7a) and cut into 25 mm wide samples, as shown in Figure 4.20b. Additionally, a hole is drilled for the mounting in the test setup.

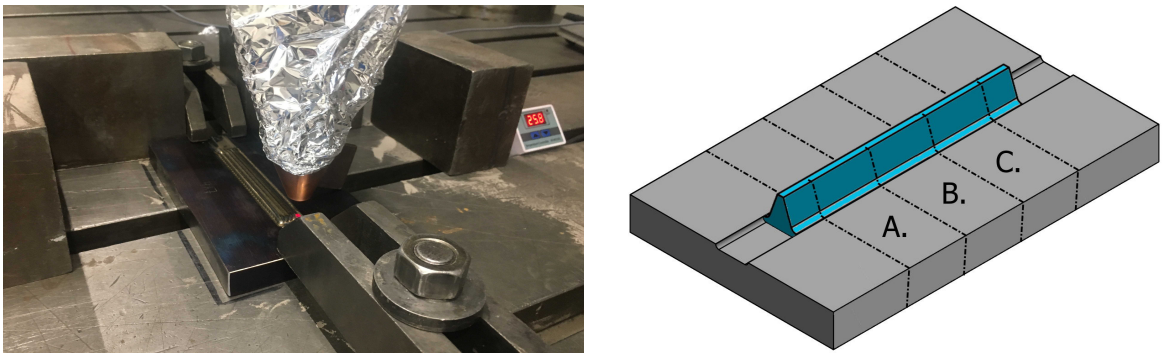

(a) (b)

Figure 4.20: (a) Setup of the substrate and laser head during deposition. The digital indicator on the right shows the temperature of the substrate. (b) Schematic view of the resulting structure of the (blue) and the three samples.

From this point onward, the geometry of the test specimens is similar to a gear tooth and therefore more complex compared to previous tests. Due to this complexity it is no longer possible to accurately calculate stresses and strains within the specimen without the use of Finite Element software. Hence, force and displacement are used to display further results, leading to the use of yield force and ultimate force instead of yield strength and ultimate tensile strength, respectively.

4.2.1. Interpass Temperature

Before comparing a built up structure with a carburized reference tooth, the influence of the interpass temperature during the deposition is investigated to ensure the core material of the tooth has the optimal mechanical properties.

Thermal history plays a dominant role in the quality of deposited structures of Inconel 718. By adjusting the interpass temperature the cooling rates can be controlled. Interpass temperature is defined as the maximum allowed temperature of the deposited structure at which a subsequent layer can be initiated. A lower interpass temperature is directly related to an increase in the solidification rate due to a relatively larger heat sink. The mechanical properties of deposited Inconel 718 is affected by the solidification rate — and interpass temperature — in three ways:

- Low solidification rate: This is related to the formation of large dendrites [35, 36]. During solidification, the presence of solid nuclei inside the undercooled liquid initiate the growth of γ phase dendrites, which predominantly grow towards the deposition direction and form columnar structures. These dendrites are detrimental for the performance of the deposited material due to the formation of large dislocation planes [37].
- Liquation cracking: This failure mode is related to the thermal stresses induced by the process combined with metallurgical defects. Research has shown a reduced chance of cracking can be obtained by an increase in cooling rate [38, 39].
- Laves phases: The presence of Laves phases is common in laser deposited nickel super alloys. These intermetallic particles, formed during low cooling rates and tend to impair the performance of the material due to its brittle and hard nature [40].

According to three considerations listed above, it is expected that a lower interpass temperature will lead to a higher yield strengths and a ultimate tensile strengths of the deposited structures. This is investigated by depositing a multilayer tooth structure while controlling the temperature in the structure. During deposition, the interpass temperature is measured before depositing a new layer. A temperature sensor is placed at 50 mm from the centerline of the tooth, according to welding standards [41]. The sensor triggers a relay which is connected with the LMD setup. The three considered interpass temperatures used in this step are: 80°C, 100°C and a continuous deposition. It was found that a continuous (i.e. no additional waiting time between subsequent layers) laser deposition resulted in a maximum interpass temperature of 130°C. The resulting samples are shown in Figure 4.21.

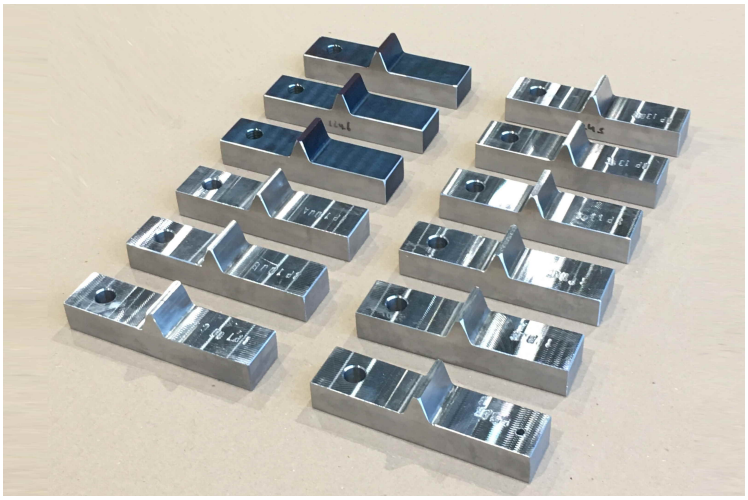

Figure 4.21: Static load test specimens deposited with different interpass temperature. The darker specimens are the carburized 18CrNiMo7-6 reference samples, which will be tested later in the research.

Figure 4.22 shows a comparison between the different fracture surfaces of the teeth. For every interpass temperature signs of non-homogeneity can be observed in the jagged fracture surfaces. However, it is seen that the higher interpass temperature (Figure 4.22c) leads to a more distinctive pattern with alternating brittle and ductile fracture, whereas a lower interpass temperature (Figure 4.22a) clearly results in a more uniform fracture surface.

(a) (b) (c)

Figure 4.22: Top view of the static load test specimens showing the fracture surfaces after testing. Used interpass temperatures are: (a) 80°C, (b) 100°C and (c) 130°C

The resulting mechanical properties from the static load test for specimens built with different interpass temperatures are depicted in Figure 4.23a and 4.23b. It can be seen that a lower interpass temperature results in a slightly higher yield force and ultimate force. This improvement is attributed to a lower amount of liquation cracking and a higher solidification rate. This implies that higher cooling rates in the deposition of Inconel 718 lead to an increase in the resulting mechanical properties.

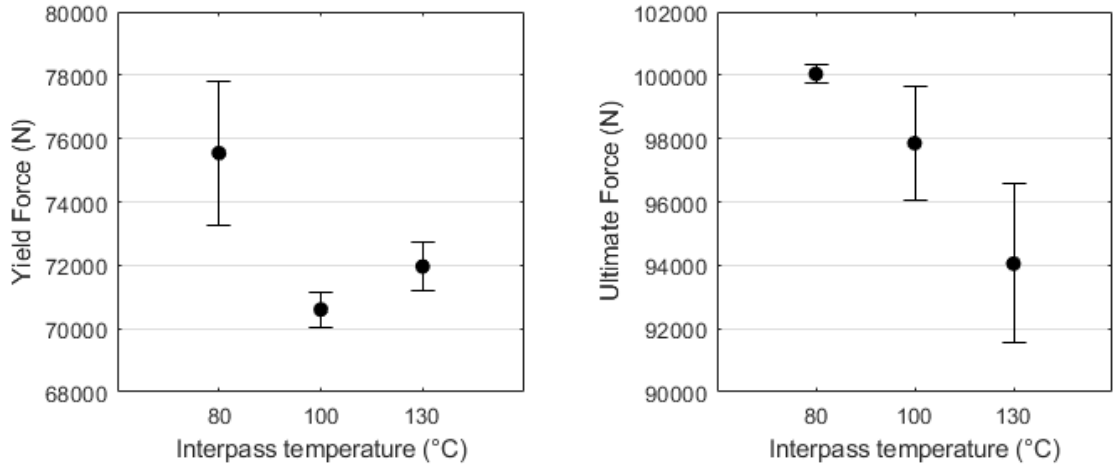

(a) (b)

Figure 4.23: Averages and standard deviation of the yield force and ultimate force for different interpass temperatures. Each point represents a total of 3 tests.

Furthermore, it is found that the fracture mechanism does not correspond with a regular tooth failure. Tooth breakage typically is initiated at the flank or root of the tooth. It can be seen that the top of the structure has broken off at the contact point with the press rod, where a high point load is introduced by the sharp edge of the press rod. In this case, the combination of local contact stress and shear stress lead to a cutting of the top. This premature failure mechanism, however, does not occur in a typical load cycle of a gear, since the involute flank shapes generate a more distributed load on the gear flank.

Additional testing: Press Rod Geometry

To exclude any affect of the press rod geometry, additional testing is performed. A rounder edge was designed to create a more distributed contact point and prevent the top of the tooth structures from failing under local contact stresses. Figure 4.24a and Figure 4.24d show the different geometries of the press rod. New specimens are prepared with the deposition parameters from Table 4.11 and an interpass temperature of 80°C. Subsequently, the samples are tested with a static load test.

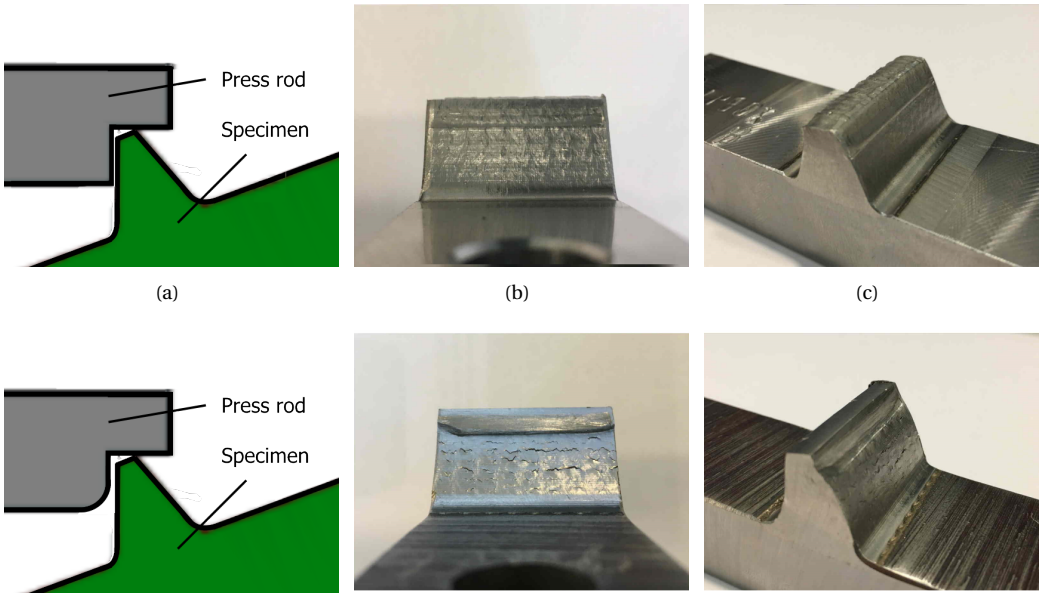

(a) (b) (c)

(d) (e) (f)

Figure 4.24: Schematic overview of the (a) sharp and (d) round press rod used in the static load test and pictures of the corresponding specimens after testing. Waviness and cracks is shown at the flanks in (b) and (e). (c) and (f) show the deformed structures.

The deformed samples after the static load test are shown in Figure 4.24b, c, e and f. A significant difference in outcome is observed. The round press rod has eliminated the cutting of the tip prevented the structure from breaking off the base even when the maximum force of the setup of approximately 215 kN was applied. Figure 4.26a shows that after a certain point the force continues to increase while the displacement hardly changes. This mechanical behavior is caused by the excessive deformation of the tooth, changing the geometry and stresses at different locations. Initially, the stiffness of the tooth is mainly determined by the bending stiffness of a cantilever beam, shown in Formula 2.2. When large plastic deformation occurs, the moment arm L is significantly reduced until the point where it approaches zero, as illustrated in Figure 4.25. At this particular point the stiffness of the structure is determined by the compressive stiffness of the material, which is significantly higher than the initial bending stiffness. Since the slope of the force-displacement graphs prior to the compressive behavior is approaching zero, it is assumed that the structure is close to breakage. Using the force at this point as the ultimate force makes it able to compare different results.

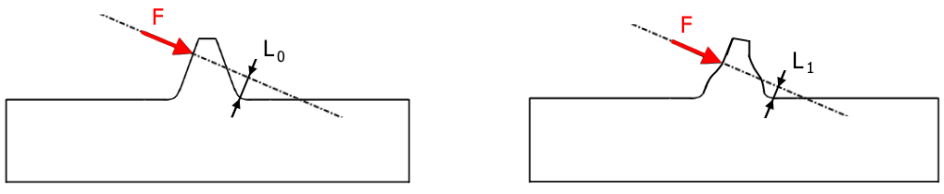

(a) (b)

Figure 4.25: The tooth shape during testing in the (a) undeformed state with the initial moment arm L_0 and (b) the deformed state with the reduced moment arm L_1 .

The resulting forces of the test are shown in the bar chart in Figure 4.26b. It is seen that the structures tested with a round press rod exhibit a higher yield and ultimate strength. This effect is attributed to the more evenly distribution of the extreme contact forces.

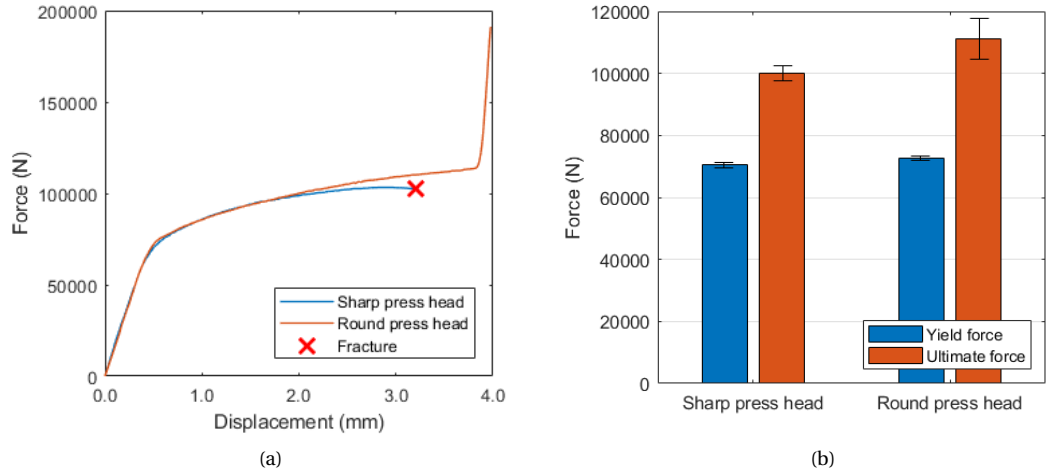

Figure 4.26: Static load test results using different rod shapes. (a) Force-displacement graph showing the mechanical behavior. (b) Averages and standard deviation of the yield force and ultimate force. Each bar represents a total of 3 tests.

Two more important facts stand out after testing with the rounded press rod. The first thing that should be mentioned is the superior bonding between the deposited structure and the case hardened steel. Even at the maximum load level of the setup, no signs of deformation or cracks at the interface between the deposited structure and the substrate are visible. This eliminates the risk of tooth detachment after repair. Secondly, looking at the flanks in Figure 4.24e and f, a non-homogeneous behavior is observed. Distinct tracks and layers are revealed by waviness and cracks at the surface. Nevertheless, the structure does not fail, proving for a very high toughness and resistance to crack propagation. The following research will be done with the adjusted rounded press rod.

4.2.2. Hard flank

It is seen that a tooth structure is built up with excellent toughness properties. However, the tooth is not comparable to a case hardened tooth, since it does not contain a hard layer to increase its wear resistance when in service. Before comparing the resulting structure from the described repair technique to a case hardened gear tooth, the influence of added hard flanks on the mechanical properties on a deposited tooth structure is studied. The deposition of a hard layer involves reheating of the previously deposited Inconel 718 core material. Even though Inconel 718 is known for its high melting point and heat resistance, the heat input generated by the addition of a new flank layer will most likely change the microstructure and mechanical properties. Another effect that could occur is the formation of unwanted particles with a possible detrimental effect, since a different material is bonded — and therefore mixed with — to the Inconel 718. The goal of this step is to discover possible effects of the deposition of a hard flank on the performance of the core structure.

To investigate the effects on the tooth structure, the core material is deposited using the parameters shown in Table 4.11. After milling it into the tooth shape as shown in Figure 4.20b an additional 1 mm of the flanks is removed, corresponding to the typical effective case depth for the chosen geometry. On each flank, 2 layers of hard material are deposited in a crosswise pattern to make the tooth more wear resistant. For the flank material, NT NI-60 is selected. This material, like Inconel 718, is used because it is a nickel based alloy, reducing the risks at the formation of unwanted particles. The theoretical hardness after deposition is 60 HRC, by far exceeding the desired 50 HRC at the effective case depth. The material composition is shown in Table 4.12. The best settings for depositing a hard layer on the flanks is a challenge at itself. The influence of parameters affecting the quality of the hard flank layer is not investigated in this research but based on the in-house parameters for a single layer of NT-NI60 are used. The parameters are shown in Table 4.13. After the deposition the tooth is milled to the original tooth shape, cut into 3 specimens and tested in the static load

test setup.

Table 4.12: Chemical composition of NT NI-60.

Material	Ni	C	Si	B	Cr	Fe
NT NI-60	Balance	1.0	4.0	3.2	15.0	4.0

Table 4.13: Primary deposition parameters for the hard flank material.

Parameter	Value
Laser power	1400 W
Scanning speed	200 mm/min
Deposition rate	2.7 g/min

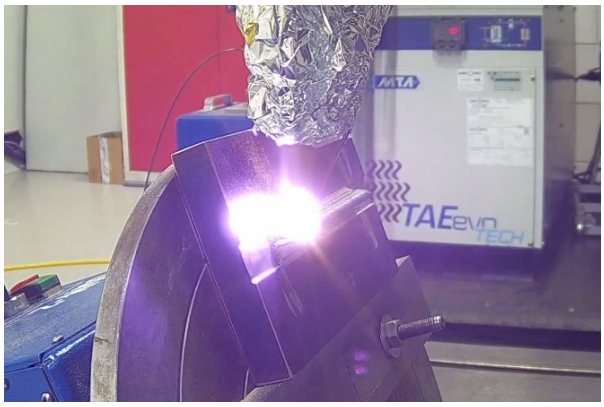

Figure 4.27: Setup during deposition of the hard flank material, the substrate is placed on a 20° tilted table to achieve a perpendicular deposition.

The static load test results for specimens with and without a hard flank are depicted in Figure 4.28. According to the bar chart diagram in Figure 4.28b, an increase in yield strength is noted when a hard flank is added. This increase is attributed to the hard flank material: a harder material typically shows higher yield strength. However, higher strength is accompanied with less ductility. This decrease in ductility is observed in the force-displacement diagram (Figure 4.28a). A non-smoothness — note that this is not the yielding plateau which is typically observed in carbon steels — is observed after yielding.

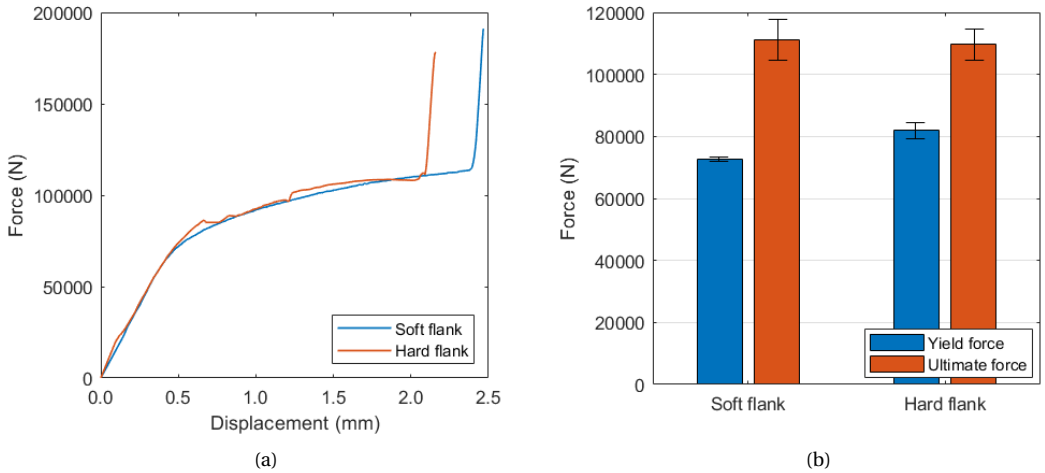

(a) (b)

Figure 4.28: Static load test results for specimens with and without a deposited hard flank. (a) Force-displacement graph showing the cracking zone and compressive behavior. (b) Averages and standard deviation of the yield force and ultimate force. Each bar represents a total of 3 tests.

The shown behavior can be explained by looking at the specimen shown in Figure 4.29. The specimens with the deposited hard flanks show cracking at the surface. The flank material has failed by brittle fracture but the crack propagation was stopped at the tough core material. After the cracking the specimens continue

with a mechanical behavior similar to the samples without a hard flank. Despite cracked flanks, reducing the effective horizontal cross sectional area of the tooth, no failure occurred. It is therefore concluded that reheating due to the deposition of hard material on the flanks does not have detrimental effects but even contributes to the mechanical properties of the core and the tooth in general.

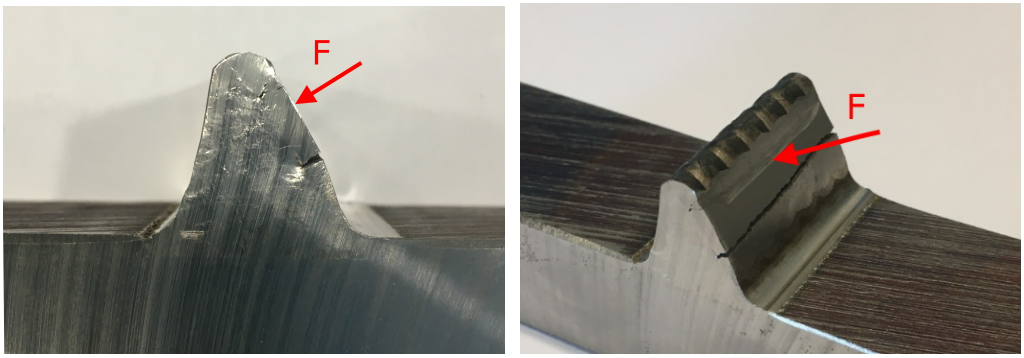

(a) (b)

Figure 4.29: Pictures of the test specimens with an additional hard flank after a static load testing, showing the direction of force during the test. A crack is initiated at the flank and stopped at the core material.

4.2.3. Final Comparison

The final part of this research studies the plastic and elastic behavior of a traditionally produced reference tooth and a deposited tooth using LMD. The reference tooth consists of a 18CrNiMo7-6 block of steel, machined to the dimensions shown in Figure 3.7a to create a 200 mm long tooth. Subsequently, the steel is case hardened and a total of 3 static load test samples is cut out. The mechanical performance of the reference tooth is compared to a deposited tooth including a hard outer layer on a case hardened base. Figure 4.30a shows the resulting composition of materials in the cross section of the built up tooth. It is seen that the desired material composition is achieved: an Inconel 718 core and root combined with tooth flanks made of NT-NI60. To verify the wear resistance of the hard flank layer, hardness testing is performed. The results are shown in Figure 4.30b. It is seen that the desired effective hardness of 50 HRC is not shown across the entire layer. Especially at the dilution zone, where the Hertzian contact forces reach, sufficient hardness is critical. Future research on the deposition parameters of the outer layer is recommended.

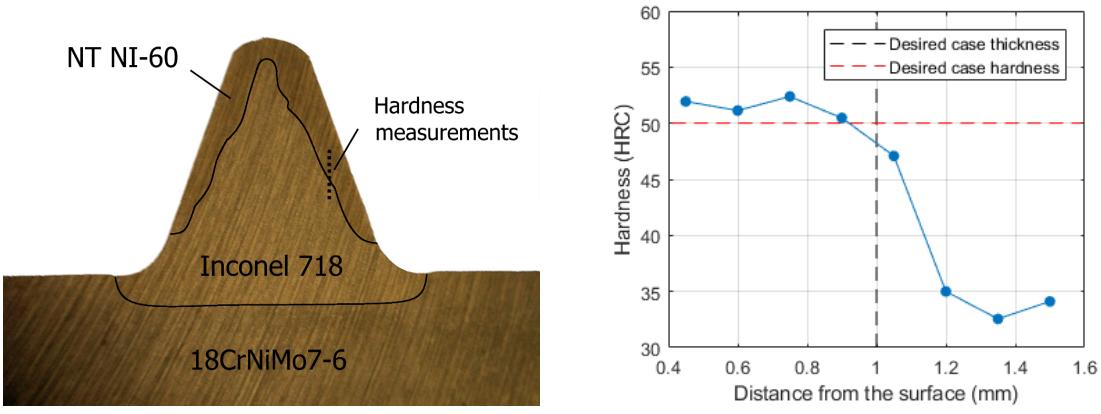

(a) (b)

Figure 4.30: (a) Macrophoto showing the different materials in the deposited tooth after grinding and etching with cleaning vinegar. Note that the colors are not related to the hardness of the material. The location of the hardness tests is shown as well. (b) The hardness profile from the hard layer to the core material relative to the distance to the outer surface of the tooth.

A total of 6 samples is tested with a static load test. The results are shown in Table 4.14 and Figure 4.31. As

stated, the idea behind this research is to be able to replace a broken tooth and extend the service life of a damaged gear. This means that the replaced structure should be able to withstand similar loading conditions without showing any signs of deformation. Therefore the most interesting mechanical properties are those within the elastic range of the material. It is noted that the yield force of the deposited structure reached over 50% of the yield force of the reference tooth. Furthermore, it can be observed that both structures show very dissimilar mechanical behavior. Especially when the teeth is loaded beyond its yield point, large differences are noted. It is seen that the deposited structure is subject to large plastic deformation before showing compressive behavior without breakage, whereas the reference tooth shows less yielding before sudden brittle breakage.

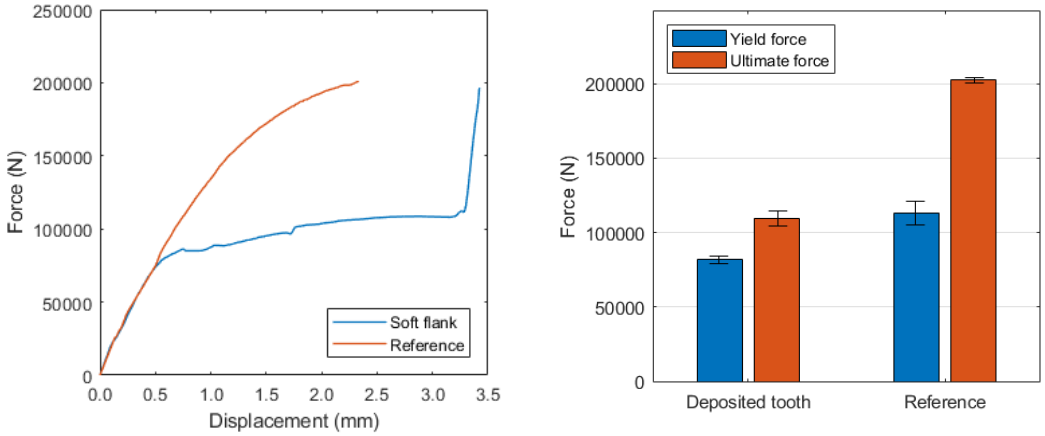

Figure 4.31: (a) Force-displacement graph and (b) averages and standard deviation of the yield force and ultimate force for the deposited tooth structure and the reference tooth. Each bar represents a total of 3 tests.

A reason for the inferior mechanical properties of the deposited structure is found in the previous results. Here, a non-homogeneous microstructure was observed due to the irregular deformation of the flanks. These local weak parts are created by the layer-by-layer production method of LMD. This suggests that the mechanical properties — the yield and ultimate tensile strength in particular — of the deposited Inconel 718 structure do not match the properties of its bulk material. Therefore, research on further strengthening of Inconel 718 is required. Another important factor regarding the outcome of the comparison of the deposited and the reference tooth is the difference in internal residual stress in the structures. The outer layer of the reference tooth is typically loaded wit compressive stress due to the carburization process. The flank layer of the deposited tooth, however, is expected to be subject to thermal tensile stresses, causing premature failure of the hard flank layer. It is expected that the reduction of thermal stresses in this material will significantly contribute to the performance of the remanufactured tooth.

Table 4.14: Final static load test results for deposited structures with and without a hard flank layer and a case hardened 18CrNiMo7-6 tooth.

	Yield force kN	Ultimate force kN
Soft flank	73 ± 0.8	111 ± 6.7
Hard flank	82 ± 2.4	109 ± 4.8
Reference	131 ± 7.8	202 ± 1.6

It should be noted that the presented results in this study only hold for a static situation. Hence, it is suggested that the dynamic behavior, fatigue limits and impact resistance of the remanufactured tooth are evaluated in further research.

5

Conclusion

AM has gained momentum in the past decades, causing a significant reduction in costs and a more environmental friendly way of part repair. Nevertheless, a lack of knowledge with respect to the repair techniques for industrial gears has led to the urge for a solution. An elaborate study is laid down to develop a new method for the replacement of a broken tooth from a carburized gear with the use of LMD.

Where two worlds are combined, often new opportunities and risks emerge. An analysis of the functions of a gear tooth is combined with the pitfalls of LMD as repair method. This served as the basis for an extensive multi-step research, with each step focusing on different failure mechanisms. The fundamental part of the study shows the effects of different deposition parameters on the properties of a laser aided deposited structure of Inconel 718. Large effects were found with the adjustment of the thermal history and scanning pattern. A custom load test setup is developed to mimic the static bending and breakage of single tooth specimens built under varying circumstances. Doubts about carbon concentrations leading to tooth detachment were taken away by the unaffected interface between the tooth and a carburized substrate. It is also shown that the addition of a hard flank layer does not have any adverse effects on a deposited Inconel 718 tooth core.

When a structure including hard flanks is compared to a traditionally manufactured hardened gear tooth, inferior static mechanical properties are observed. This implies that the remanufactured tooth is not capable to transmit the full power of a gear. However, high ductility and extreme resistance to crack propagation have raised high expectations regarding the fatigue and impact properties of deposited structures. Concluding it can be said that the presented repair method is not able to restore the mechanical performance of a gear to its original state. Nonetheless, for gear mechanisms that are allowed to run at a lower power rate, it is seen as a promising temporary solution to reduce high costs and downtime.

5.1. Recommendations

Although the presented study for has led to a promising repair method, it is not applicable as it is now. Before applying it to actual gear, further investigation is recommended on the following subjects:

- Investigation on the hard flank material. The performance of the hard flank layer is deducted from a single hardness profile. Future research of the flank material should be performed, including thorough hardness and wear resistance tests and research on the homogeneity.
- Investigation on the core material. The loaded Inconel 718 structures show local deformations at the surface. An increase of material properties is expected when this non-homogeneity is reduced.
- Additional dynamic, impact and fatigue testing of the tooth. So far only static mechanical behavior is measured. Eventually, a validation of the results through testing on a carburized gear under realistic working conditions is advised before applying the repair method.
- Research on the feasibility of the repair technique for softer types of gear. These gears typically do not require the extreme mechanical properties of industrial gears and could therefore benefit from the repair technique as it is now.

A

Static Load Testing Setup

At a certain point in the research on tooth repair, standard material tests are no longer useful. To examine the mechanical behavior of a repaired tooth, it is favorable to have a good method to compare the results of used repair technique to an existing carburized gear. Because manufacturing and testing on actual gears is not time and cost-effective a special testing setup is developed.

It is desired to keep the tests as simple as possible. Figure A.1a shows geometry of the single tooth rack test specimen. The chosen width for the specimen is 25 mm. For complexity reasons considering the fabrication of the specimen, the flanks of the tooth are chosen to be straight with a 20° pressure angle, similar to a regular spur gear. A hole is added to mount the specimen in the tilted holder with an M10 bolt. To avoid any influence by the geometry, all static load tests are performed with specimens of these dimensions.

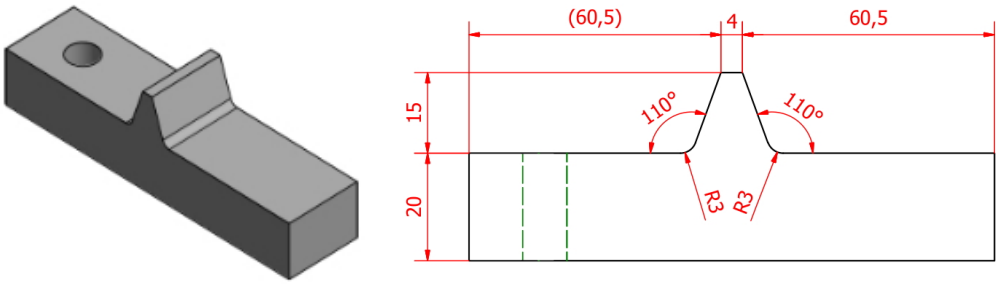

(a) (b)

Figure A.1: (a) Schematic drawing and (b) dimensions in mm of the single tooth rack test specimen for static testing.

To make sure the setup is capable of generating enough force to break the test specimen, a simple calculation is made. This is done by using the Lewis bending stress equation for gears, which states:

$$W_t = \frac{\sigma F Y}{D_P}, \tag{A.1}$$

with

$$D_P = 1/m, \tag{A.2}$$

where W_t is the applied load, σ the maximum stress in the tooth, F the face width of the tooth, Y the Lewis Factor and m the module. The ultimate tensile stress of the carburized case is estimated at 2300 MPa. The face

width, Lewis factor and module of the chosen tooth rack geometry equal 25 mm, 0.484 and 6.67, respectively. Filling in these values gives a maximum load of approximately 185 kN.

The setup consists of steel frame including a hydraulic cylinder, mounting stand to hold the specimen at an angle of 20° and hardened press rod. A hardened press rod is mounted into the hydraulic cylinder. It is designed to apply the load on 70% of the height of the tooth. This corresponds roughly with the HPSTC. By applying the force at this critical point, the highest stresses during a full loading cycle are mimicked. The used Enerpac cylinder generates a force up to 215 kN and is attached to an Enerpac Hydraulic pump including a Hawe PWM controllable proportional valve and digital pressure transmitter.

All components are designed for a working pressure of up to 700 bar. The valve and transmitter are connected to a Input/Output module of National Instruments and is read out and controlled using a laptop. The displacement is measured with a TESA Digital dial gauge with a measuring range and resolution of 13 mm and 0.01 mm respectively. The gauge is connected by cable through USB to the same laptop and can be read with a frequency of 8 Hz. A full schematic overview of the is shown in Figure A.2. The final setup and a more detailed overview are depicted in Figure A.3 and A.4.

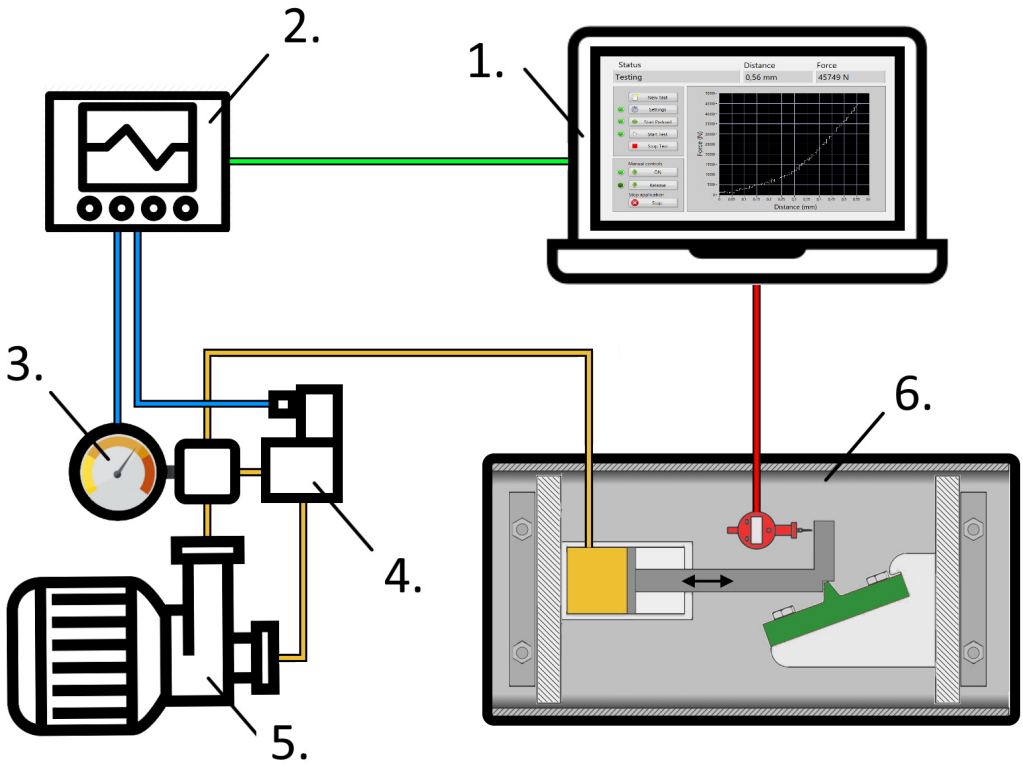

Figure A.2: Schematic diagram of the full system with 1. Laptop/computer, 2. I/O module, 3. Digital pressure transmitter, 4. Proportional valve, 5. Hydraulic pump and 6. Test frame.

Using LabView a program was designed to create a user interface from where the tests can be started and monitored. The system is PI-controlled using the pressure as feedback. Therefore, it is possible to manually enter the desired force rate. During a test, the time, pressure and displacement are logged every 200 ms. Subsequently, the pressure is converted to a force and all data is saved in a .csv data format for data processing purposes. An example of the test screen is shown in Figure A.5. After testing, raw data is imported from excel spreadsheets, filtered and processed with Matlab. The filtered data is used to calculate the yield force and ultimate tensile strength.

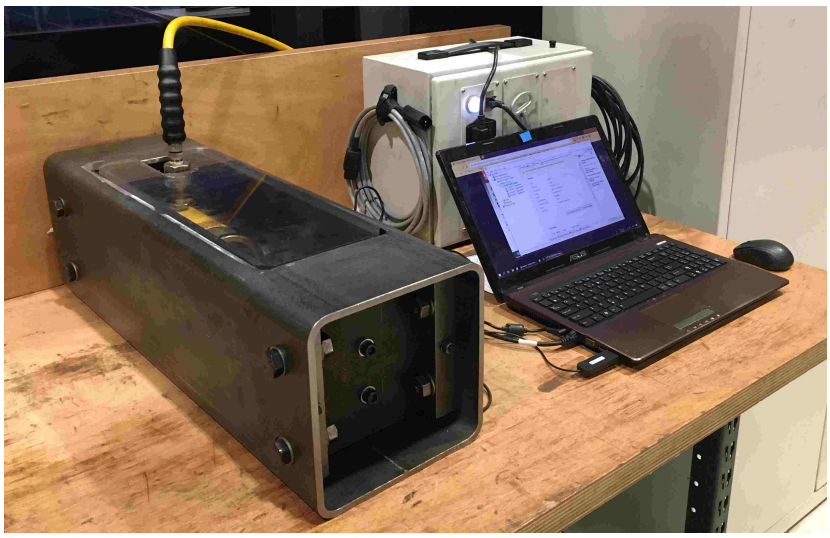

Figure A.3: Overview of the test setup (hydraulic pump and valve not in picture) as used in this research.

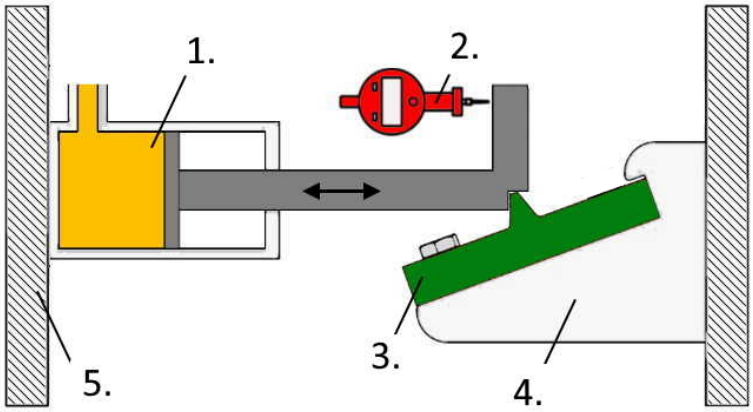

Figure A.4: Schematic drawing of the test frame with 1. Hydraulic cylinder, 2. Digital dial gauge, 3. Test specimen, 4. Mounting stand and 5. Rigid frame.

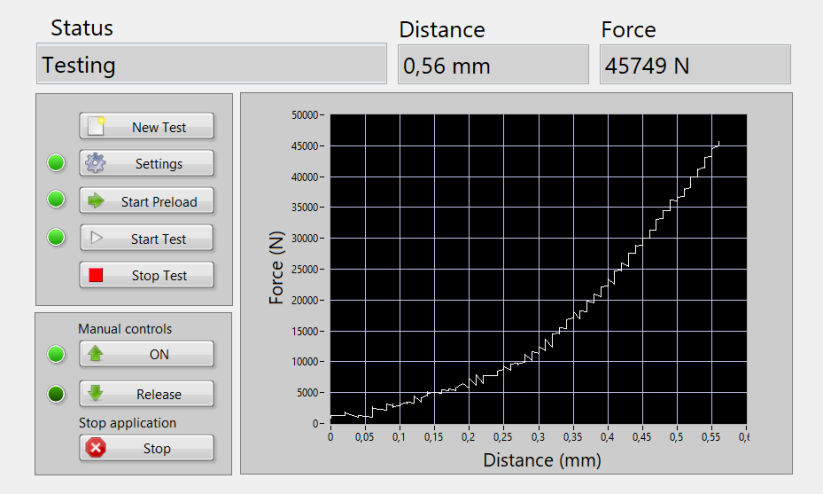

Figure A.5: Test screen during testing, showing the current status of the system (top) and a force-displacement graph (right). A control panel (left) is designed to manually start and stop the test at all times.

Bibliography

[1] M. Fischedick. *Climate Change 2014: Mitigation of Climate Change. Contribution of Working Group III to the Fifth Assessment Report of the Intergovernmental Panel on Climate Change*, chapter Industry, pages 739–810. Cambridge University Press, 2014.

[2] Rasheedat M. Mahamood, Esther T. Akinlabi, and Moses G. Owolabi. *Laser Metal Deposition Process for Product Remanufacturing*, pages 267–291. Springer International Publishing, Cham, 2017.

[3] J. M. Wilson, C. Piya, Y. C. Shin, F. Zhao, and K. Ramani. Remanufacturing of turbine blades by laser direct deposition with its energy and environmental impact analysis. *Journal of Cleaner Production*, 80:170 – 178, 2014.

[4] W. R. Morrow, H. Qi, I. Kim, J. Mazumder, and S. J. Skerlos. Environmental aspects of laser-based and conventional tool and die manufacturing. *Journal of Cleaner Production*, 15(10):932 – 943, 2007.

[5] P. Bendeich, N. Alam, M. Brandt, D. Carr, K. Short, R. Blevins, C. Curfs, O. Kirstein, G. Atkinson, T. Holden, and R. Rogge. Residual stress measurements in laser clad repaired low pressure turbine blades for the power industry. *Materials Science and Engineering: A*, 437(1):70 – 74, 2006. Neutron Diffraction Characterization of Mechanical Behavior.

[6] J. M. Lourenço, S. Da Sun, K. Sharp, V. Luzin, A. N. Klein, C. H. Wang, and M. Brandt. Fatigue and fracture behavior of laser clad repair of aermet® 100 ultra-high strength steel. *International Journal of Fatigue*, 85:18 – 30, 2016.

[7] S. Tumuluri, P. Murugeshan, R. K. Mishra, and V. V. Subrahmanyam. Application of direct metal deposition process for failure prevention of oil pump gear shaft in an aero engine. *Journal of Failure Analysis and Prevention*, 17(4):788–795, Aug 2017.

[8] E. Díaz, M. J. Tobar, A. Yáñez, J. García, and J. Taibo. Laser powder welding with a co-based alloy for repairing steam circuit components in thermal power stations. *Physics Procedia*, 5:349 – 358, 2010. Laser Assisted Net Shape Engineering 6, Proceedings of the LANE 2010, Part 1.

[9] J. R. Davis. *Gear materials, properties, and manufacture*. ASM International, 2005.

[10] T. Tobie, F. Hippenstiel, and H. Mohrbacher. Optimizing gear performance by alloy modification of carburizing steels. *Metals*, 7(10), 2017.

[11] D. Walton and A. J. Goodwin. The wear of unlubricated metallic spur gears. *Wear*, 222(2):103 – 113, 1998.

[12] M. J. Schneider and M. S. Chatterjee. *Introduction to Surface Hardening of Steels*, pages 389–398. ASM Actualites Cardiologiques et Angeiologiques Internationales, 2013.

[13] C.W. Hull. Apparatus for production of three-dimensional objects by stereolithography, March 11 1986. US Patent 4,575,330.

[14] C. Atwood, M. Ensz, D. Greene, M. Griffith, L. Harwell, D. Reckaway, T. Romero, E. Schlienger, and J. Smugeresky. A tool for direct fabrication of metal parts. *Laser Engineered Net Shaping (LENS(TM))*, 1998.

[15] S. M. Thompson, L. Bian, N. Shamsaei, and A. Yadollahi. An overview of direct laser deposition for additive manufacturing; part i: Transport phenomena, modeling and diagnostics. *Additive Manufacturing*, 8:36–62, 2015.

[16] J. M. Flynn, A. Shokrani, S. T. Newman, and V. Dhokia. Hybrid additive and subtractive machine tools, research and industrial developments. *International Journal of Machine Tools and Manufacture*, 101:79 – 101, 2016.

[17] F. Brückner and C. Leyens. *Hybrid laser manufacturing*, chapter 3, pages 79 – 97. Woodhead Publishing Series in Electronic and Optical Materials. Woodhead Publishing, 2017.

[18] K. Salonitis, L. D'Alvise, B. Schoinochoritis, and D. Chantzis. Additive manufacturing and post-processing simulation: laser cladding followed by high speed machining. *The International Journal of Advanced Manufacturing Technology*, 85(9):2401–2411, Aug 2016.

[19] B. Graf, S. Ammer, A. Gumenyuk, and M. Rethmeier. Design of experiments for laser metal deposition in maintenance, repair and overhaul applications. *Procedia CIRP*, 11:245 – 248, 2013. 2nd International Through-life Engineering Services Conference.

[20] F. Kahlen and A. Kar. Tensile strengths for laser-fabricated parts and similarity parameters for rapid manufacturing. *Journal of Manufacturing Science and Engineering*, 123(1):38–44, December 1999.

[21] W. Ya. *Laser Materials Interactions During Cladding: Analyses on Clad Formation, Thermal Cycles, Residual Stress and Defects*. University of Twente, 2015.

[22] H. Lee, C. H. J. Lim, M. J. Low, N. Tham, V. M. Murukeshan, and Y. Kim. Lasers in additive manufacturing: A review. *International Journal of Precision Engineering and Manufacturing-Green Technology*, 4(3):307–322, July 2017.

[23] J. Verwimp, M. Rombouts, E. Geerinckx, and F. Motmans. Applications of laser cladded wc-based wear resistant coatings. *Physics Procedia*, 12:330 – 337, 2011. Lasers in Manufacturing 2011 - Proceedings of the Sixth International WLT Conference on Lasers in Manufacturing.

[24] J. Shi and S.Q. Bai. Research on gear repairing technology by laser cladding. In *Digital Design and Manufacturing Technology III*, volume 546 of *Key Engineering Materials*, pages 40–44. Trans Tech Publications, 4 2013.

[25] A. J. Pinkerton, W. Wang, and L. Li. Component repair using laser direct metal deposition. *Proceedings of the Institution of Mechanical Engineers, Part B: Journal of Engineering Manufacture*, 222(7):827–836, 2008.

[26] J. Song, Q. Deng, C. Chen, D. Hu, and Y. Li. Rebuilding of metal components with laser cladding forming. *Applied Surface Science*, 252(22):7934 – 7940, 2006.

[27] R. M. Mahamood and E. T. Akinlabi. Effect of the scanning speed of treatment on the microstructure, microhardness, wear, and corrosion behavior of laser metal-deposited ti–6al–4v/tic composite. *Materials Science*, 53(1):76–85, Jul 2017.

[28] S. Ocylok, A. Weisheit, and I. Kelbassa. Functionally graded multi-layers by laser cladding for increased wear and corrosion protection. *Physics Procedia*, 5:359 – 367, 2010. Laser Assisted Net Shape Engineering 6, Proceedings of the LANE 2010, Part 1.

[29] J. Yu, M. Rombouts, G. Maes, and F. Motmans. Material properties of ti6al4v parts produced by laser metal deposition. *Physics Procedia*, 39:416 – 424, 2012. Laser Assisted Net shape Engineering 7 (LANE 2012).

[30] L. Nan, W. Liu, and K. Zhang. Laser remanufacturing based on the integration of reverse engineering and laser cladding. *Int. J. Comput. Appl. Technol.*, 37(2):116–124, March 2010.

[31] International Organization for Standardization. Iso 18265:2013 metallic materials — conversion of hardness values. Standard, International Organization for Standardization, Geneva, CH, 2013.

[32] International Organization for Standardization. Iso 5173:2010: Destructive tests on welds in metallic materials - bend tests. Standard, International Organization for Standardization, Geneva, CH, 2010.

[33] J. Yu, T. Jung, S. Kim, and S. Rhee. Laser welding of cast iron and carburized steel for differential gear. *Journal of Mechanical Science and Technology*, 25(11):2887–2893, 2011. 2887.

[34] International Organization for Standardization. Iso 15614-7:2016: Specification and qualification of welding procedures for metallic materials - welding procedure test - part 7: Overlay welding. Standard, International Organization for Standardization, Geneva, CH, October 2016.

[35] H. Helmer, A. Bauereiß, R.F. Singer, and C. Körner. Grain structure evolution in inconel 718 during selective electron beam melting. *Materials Science and Engineering: A*, 668:180 – 187, 2016.

[36] F. Liu, X. Lin, C. Huang, M. Song, G. Yang, J. Chen, and W. Huang. The effect of laser scanning path on microstructures and mechanical properties of laser solid formed nickel-base superalloy inconel 718. *Journal of Alloys and Compounds*, 509(13):4505 – 4509, 2011.

[37] P. Cao. Characterization of laser deposited alloy 718. Master's thesis, KTH, Materials Science and Engineering, 2016.

[38] Y. Chen, K. Zhang, J. Huang, S. Reza, E. Hosseini, and Z. Li. Characterization of heat affected zone liquation cracking in laser additive manufacturing of inconel 718. *Materials & Design*, 90:586 – 594, 2016.

[39] Y. Zhang, L. Yang, T. Chen, S. Pang, and W. Zhang. Sensitivity of liquation cracking to deposition parameters and residual stresses in laser deposited in718 alloy. *Journal of Materials Engineering and Performance*, 26:1–11, 10 2017.

[40] L. Zhu, Z. F. Xu, P. Liu, and Y. F. Gu. Effect of processing parameters on microstructure of laser solid forming inconel 718 superalloy. *Optics & Laser Technology*, 98:409 – 415, 2018.

[41] International Organization for Standardization. Iso 13916:2017: Welding - measurement of preheating temperature, interpass temperature and preheat maintenance temperature. Standard, International Organization for Standardization, Geneva, CH, 2017.